JUNE 1996

ECN-I--96-025

ECN
energy innovation

TEMPERATURE ANALYSES FOR CORVIS EXPERIMENTS WITH OXIDIC MELT

H. BRAAM
J.H. FOKKENS

The Netherlands Energy Research Foundation ECN is the leading institute in the Netherlands for energy research. ECN carries out basic and applied research in the fields of nuclear energy, fossil fuels, renewable energy sources, policy studies, environmental aspects of energy supply and the development and application of new materials.

ECN employs more than 800 staff. Contracts are obtained from the government and from national and foreign organizations and industries.

ECN's research results are published in a number of report series, each series serving a different public, from contractors to the international scientific world.

The I-series is for internal reports that contain results mainly of interest for (fellow) colleagues, principally within ECN but also for those employed elsewhere. Although these reports may not be in their final form, they may be referred to.

Het Energieonderzoek Centrum Nederland (ECN) is het centrale instituut voor onderzoek op energiegebied in Nederland. ECN verricht fundamenteel en toegepast onderzoek op het gebied van kernenergie, fossiele-energiedragers, duurzame energie, beleidsstudies, milieuaspecten van de energievoorziening en de ontwikkeling en toepassing van nieuwe materialen.

Bij ECN zijn ruim 800 medewerkers werkzaam. De opdrachten worden verkregen van de overheid en van organisaties en industrieën uit binnen- en buitenland.

De resultaten van het ECN-onderzoek worden neergelegd in diverse rapportenseries, bestemd voor verschillende doelgroepen, van opdrachtgevers tot de internationale wetenschappelijke wereld.

De I-serie is de serie interne rapporten die resultaten bevat bestemd voor de ECN-collega's, maar ook voor vakcollega's die elders werkzaam zijn. Deze rapporten hebben een minder definitief karakter, maar zijn wel refereerbaar.

Netherlands Energy Research Foundation ECN
P.O. Box 1
NL-1755 ZG Petten
the Netherlands
Telephone : +31 2246 49 49
Fax : +31 2246 44 80

This report is available on remittance of Dfl. 35 to:
ECN, Facility Services,
Petten, the Netherlands
Postbank account No. 3977703.
Please quote the report number.

Energieonderzoek Centrum Nederland
Postbus 1
1755 ZG Petten
Telefoon : (02246) 49 49
Fax : (02246) 44 80

Dit rapport is te verkrijgen door het overmaken van f 35,-- op girorekening 3977703 ten name van:
ECN, Faciliteiten
te Petten
onder vermelding van het rapportnummer.

JUNE 1996

KS002065149
R: FI
DE009064321

ECN-I--96-025

DE009064321

TEMPERATURE ANALYSES FOR CORVIS EXPERIMENTS WITH OXIDIC MELT

H. BRAAM
J.H. FOKKENS

Revisions		
A	Draft for review	May 1996
1	Final	June 1996

Made by H. Braam J.H. Fokkens	**Approved by** J. Prij	ECN Nuclear Energy Structural and Risk Analysis
Checked by J. Prij	**Issued** H. Braam	

This report contains the work performed as part of the projects 1702 (1995) and 7.1067 (1996) of ECN Nuclear Energy.

CONTENTS

1. INTRODUCTION

During a severe accident in a light water reactor molten core material, or corium, will move downwards and might come in direct contact with the Reactor Pressure Vessel (RPV) Lower Head. The project CORVIS (Corium Reactor Vessel Interaction Studies) is a research programme for the experimental and analytical investigation of possible failure modes of the RPV during a severe accident. To investigate a core melt down experimentally a melt produced with a thermite charge is poured into the experimental test vessel. After the melt has flowed into the test vessel an electric arc heater is placed in the corium for a sustained heating of the melt. In the analytical part of CORVIS a computational model of RPV lower head failure will be developed. This requires both thermal and structural analyses.

The thermal analyses include heat conduction, heat convection, heat input and phase changes. When the corium is in the liquid phase a strong heat transport by convection might be present. To avoid extensive fluid flow calculations a solid material conduction based model was introduced in the temperature analyses for the CORVIS 01/6 experiment [1]. To simulate heat transfer by convection in a solid element conduction model a modified heat transfer coefficient was defined. Above the melting temperature of the corium the heat transfer coefficient was increased to a very high value. This model showed very good agreement between measured and calculated temperatures in the bottom plate. However, the temperature distribution in the melt was almost uniform.

In experiment 01/6 the bottom plate was in contact with an iron melt and in the analyses a perfect contact between melt and bottom plate was assumed. For an oxidic melt it is expected that crust formation will take place, which will strongly influence the heat transfer from the melt to the bottom plate. The model with a jump in the conductivity showed no or only a very small temperature gradient in the melt and is not suitable for this reason to simulate crust formation properly. To simulate crust formation in a solid element model a new relation for melt convection simulation is considered. With the true conductivity as base a number of temperature dependent multiplier curves are investigated. In order to capture accelerating heat transfer, the appropriate form seems to be a power law for the conductivity multiplier. To study the influence of this conductivity multiplier on the crust formation and on the temperature distribution a number of Finite Element (FE) calculations were made with the general purpose FE-code MARC [2]

For an iron melt a perfect contact between the melt and the bottom plate was assumed, since these are congruent materials. For an oxidic melt it is expected that the wetting will not be that good, so in the calculation model a heat resistance has to be included at the interface of melt and bottom. A number of FE-analyses are made with so called heat link elements with varying heat resistance to study the influence of this heat resistance on the temperature distribution in the bottom plate and in the melt near the interface.

2. MODEL DESCRIPTION

2.1 Geometry

The thermal calculations are made with the setup of CORVIS experiment 01/8, because the geometry of this experiment is representative for the future experiments with an oxidic melt. The hole in the bottom plate is omitted, since the purpose of this study is to develop a model for crust formation and to investigate heat resistance effects of the interface between corium and bottom plate. The geometry and the dimensions of the configuration are shown schematically in Figure 2.1. The experimental test vessel can be specified by the following data:

- Bottom plate: 840 mm diameter, 100 mm thickness;
- Vessel wall: 800 mm inner diameter, 840 mm outer diameter, 1200 mm height;
- Magnesital insulation: 600 mm inner diameter, 800 mm outer diameter, 1200 mm height;
- Heater: 356 mm outer diameter.

The melt consists of 484 kg oxidic material. At the initial temperature of 2200 °C the density of the melt is 2851 kg m^{-3}, so the level of the melt above the bottom plate equals 845 mm.

2.2 Assumptions

The following assumptions are made for the thermal analyses.

- The initial temperature of the bottom plate, the vessel wall and the insulation is 300 °C.
- The initial temperature of the melt is 2200 °C.
- The melt consists of 484 kg Al_2O_3.
- Perfect contact is assumed between melt and insulation, since these are congruent materials.
- Heat transfer to the surrounding will occur at the outside of the vessel wall and the bottom plate due to convection and radiation. From the inside of the insulation above the melt and from the surface of the melt no heat transfer will occur.
- Heat resistance between insulation and vessel wall will be neglected, in order not to further complicate the calculations, since this effect is rather small at the expected temperatures in this region.
- The effective arc heating power is assumed to be 120 kW and an adiabatic boundary condition on the interface between electrode and melt is assumed.
- The produced heat from the electrode is assumed to transfer into the oxidic melt at the bottom of the electrode uniformly distributed over a circular area with a diameter of 356 mm.
- The distance between the heater and the bottom plate is 150 mm.
- The thermal material properties for the bottom plate and the vessel wall are the same as for steel defined in [1].
- An axisymmetric thermal loading is assumed.

2.3 Material properties

The material properties used for the thermal analyses are given in Table 2.1 - Table 2.11. These properties are based on data presented in [1].

Outer wall and bottom plate

Table 2.1 *Density* ρ

Temperature [°C]	ρ [kg m^{-3}]
0	7800
3000	6500

Table 2.2 *Specific heat capacity c*

Temperature [°C]	*c* [J kg^{-1} $°C^{-1}$]
0	525
400	627
710	1074
800	2013
805	525
1400	903
3000	1000

Table 2.3 *Thermal conductivity* λ

Temperature [°C]	λ [W m^{-1} $°C^{-1}$]
0	60
625	38
800	30
1540	40
3000	40

Table 2.4 *Melting/freezing temperature, Latent heat*

Melting/freezing temperature [°C]	1540
Latent heat[J kg^{-1}]	213000

Al_2O_3 melt

Table 2.5 *Density* ρ

Temperature [°C]	ρ [kg m^{-3}]
0	4000
2040	3800
2060	3000
3000	2000

Table 2.6 *Specific heat capacity c*

Temperature [°C]	c [J kg^{-1} °C^{-1}]
0	795
200	1038
2000	1457
2050	1279
3000	1500

Table 2.7 *Thermal conductivity* λ

Temperature [°C]	λ [W m^{-1} °C^{-1}]
400	60
1300	5
2050	9
2300	16
2400	25
3000	40

Table 2.8 *Melting/freezing temperature, latent heat*

Melting/freezing temperature [°C]	2050
Latent heat [J kg^{-1}]	1120000

Magnesital insulation

Table 2.9 *Density* ρ

Temperature [°C]	ρ [kg m^{-3}]
0	2800
3000	2800

Table 2.10 *Specific heat capacity c*

Temperature [°C]	c [J kg^{-1} °C^{-1}]
20	864
1000	1219
3000	1219

Table 2.11 *Thermal conductivity* λ

Temperature [°C]	λ [W m^{-1} °C^{-1}]
0	3
1000	2
3000	2

3. THE FINITE ELEMENT MODEL

Two series of FE-analyses have been performed. For the first series denoted with "PC" a perfect contact between corium and bottom plate was assumed. This series was used to study the simulation of crust formation at the bottom plate. A number of FE-analyses was made to investigate the influence of the conductivity multiplier used to simulate heat transfer by convection in a solid element.

In the second series denoted with "HL" heat link elements were introduced at the interface between corium and bottom plate. The heat resistance of the heat links has been varied in the FE-analyses to determine its influence on the temperature distribution in the bottom plate and in the melt near the interface. The heat transfer coefficient, h_{HL}, in the heat link elements has been taken both constant (temperature independent) and dependent on the temperature of the corium. In the latter case the heat transfer coefficient was defined as depicted in Figure 3.1. A low constant level in case the heat link element is in contact with corium in the solid phase and a high constant level in case of corium in the liquid phase. To avoid numerical problems the increase from the low to the high level is assumed to change linear over a traject of 20 °C. The mean temperature of the last two time increments is used to determine the heat flux rate in the heat link elements.

3.1 FE-Mesh

The finite element model of the CORVIS configuration is shown in Figure 3.2. For the "PC" series the model consists of 5110 nodal points and 4893 elements of MARC type 40. The FE-mesh is carried out with double nodes at the transition from bottom plate to corium. In case of perfect contact these nodes are tied. MARC element type 40 is an arbitrarily distorted axisymmetric heat transfer quadrilateral element with four nodal points.

For the analyses with heat link elements 128 elements of MARC type 36 are added between the double nodes at the transition from corium to bottom plate. MARC element type 36 is a three-dimensional, two-node, heat transfer link.

3.2 Material model

The thermal material properties as described in Section 2.3 are used. Because a single melting/freezing point complicates a FE analysis with phase transitions a melting/freezing zone of 20 °C is assumed. This means that the latent heat will be set free or absorbed gradually over this zone.

The program MARC requires a constant density to be specified. For the performed analyses the density at T = 0 °C has been taken. The temperature dependency of the density is incorporated by specifying an equivalent temperature dependent specific heat c^* by:

$$c^*(T) = \frac{\rho(T)}{\rho_o} \cdot c(T)$$

with ρ_o the density at T = 0 °C. The latent heat E_1 to be entered has been adapted in a similar manner.

To simulate heat transfer by convection in a solid element a modified heat transfer coefficient λ^* is defined by:

$$\lambda^*(T) = \lambda(T) \cdot f_\lambda(T)$$

The multiplication function is defined as follows:

$$f_\lambda(T) = \begin{cases} 1 & , T \le T_m \\ 1 + \dfrac{\Lambda - 1}{(T_1 - T_m)^p} \cdot (T - T_m)^p & , T_m < T \le T_1 \end{cases}$$

with:

T_m = 2050°C (melting temperature of Al_2O_3)
T_1 = 2400°C
Λ = 50

For T > 2400 °C λ^* is interpolated linear between λ^* = 1250 for T = 2400 °C and λ^* = 10000 for T = 3000 °C. The parameter p will be varied in the FE-analyses. In Figure 3 λ^* is shown for p = 1, 2, and 3.

3.3 Loads and boundary conditions

Loading
The heat input of the electric arc is modelled as a heat flux area load, with power density of:

$$\frac{120000}{\pi \cdot 0.178^2} = 1205567.0 \quad \mathrm{Wm^{-2}}$$

This heat flux is specified at the interface between the bottom of the heater and the melt.

Initial temperatures are:
- Al_2O_3 melt : 2200°C
- nodal points at interface between melt and insulation : 2200°C
- steel vessel and insulation : 300°C
- nodal points at interface of melt and bottom in "PC" series : 1250°C
- midside nodes of heat link elements in "HL" series : 1250°C

Boundary conditions
In Figure 3.2 the applied boundary conditions are illustrated.

The heat lost by convection is determined by the heat transfer coefficient h:

$$h = a \cdot \sqrt[4]{(T - T_s)} \qquad [\mathrm{Wm^{-2}K^{-1}}]$$

with T the temperature at the outside of the vessel, a = 2.6 for the vertical outside wall and a = 3.3 for the bottom plate. The temperature of the environment T_s is assumed to be 20 °C.

The heat lost due to radiation is considered following Stefan-Boltzmann's radiation law:

$$q = 5.67\ 10^{-08} \cdot \varepsilon \cdot (T^4 - T_s^4) = h^* \cdot (T - T_s) \qquad [\mathrm{Wm^{-2}}]$$

The used emissivity coefficient ε is given in Table 3.1. The temperature of the direct environment T_s which acts as the heat sink is set to 293 K (20 °C). In MARC radiation is modelled by convection. This can be done with an equivalent heat transfer coefficient h^* defined in above equation.

Table 3.1 *Emissivity* ε

Temperature [°C]	ε
100	0.10
475	0.24
575	0.63
1000	0.83

3.4 Analyses

PC series
To simulate heat transfer by convection in a solid element model the conductivity multiplier f_λ was introduced. In the temperature range 2050 °C - 2400 °C the form of this multiplier function is a power law with parameter p. In order to investigate the influence of this parameter p analyses have been made with various values for this parameter, viz. p = 1, 3 and 5. For reasons of comparison analyses for the unmodified heat transfer coefficient and for the previous used model with a jump in the conductivity are performed also. In Table 3.2 these analyses are summarized. For these analyses a perfect contact at the interface between corium and bottom plate is assumed.

HL series
In order to estimate the influence of the heat resistance at the interface between the corium and the bottom plate a number of FE analyses have been made with heat link elements at this interface. The behaviour of these heat link elements is considered in two ways. First the heat transfer coefficient, h_{HL}, of these elements is taken independent of the corium temperature. A number of cases is

considered with heat transfer coefficients of 500 Wm^{-2} to 5000 Wm^{-2}, as specified in Table 3.3.
Second a number of analyses is made with heat link elements for which the heat transfer coefficient is dependent on the temperature of the corium as specified in Figure 3.1. The considered low and high values for the heat transfer coefficient are given in Table 3.4.

For all HL-type analyses the assumptions stated in Table 3.2 for case PC1 are used.

Table 3.2 *Survey of the analyses with perfect contact at the interface (PC series)*

Case	λ^*	
PC1	λf_λ	p = 3
PC2	λf_λ	p = 1
PC3	λf_λ	p = 5
PC4	λ	
PC5	λ	$T < 2050$ °C
	10.000	$T > 2050$ °C

Table 3.3 *Survey of the analyses with temperature independent heat link elements at the interface (HL series)*

Case	h_{HL} [Wm^{-2}]
HL1	500
HL2	1000
HL3	2500
HL4	5000

Table 3.4 *Survey of the analyses with temperature dependent heat link elements at the interface (HL series)*

Case	h_{HL} [Wm^{-2}]	
	low	high
HL12	500	1000
HL13	500	2500
HL23	1000	2500
HL24	1000	5000
HL34	2500	5000

4. RESULTS

PC series

In Figure 4.1 the calculated temperature field in the vessel wall, the bottom plate and the corium can be seen for case PC1. In this figure the temperature fields at t = 0, 60, 1000, 2000, 3000 and 4000 s are depicted. Clearly visible is the crust formation in the melt. The boundary between liquid material and solid material is at the contour line of T = 2050 °C. Also clear is the formation of a pool with molten steel in the bottom plate after 1000 s. The boundary of this pool is at the contour line of T = 1540 °C.

For a number of nodes located at the interface and at the outside of the bottom plate at a distance of r = 0, 178 and 300 mm from the centre line of the vessel the temperature as function of time is given in Figure 4.2 for case PC1. The location of the nodes considered is depicted in Figure 3.2. It can be seen that immediately after the molten Al_2O_3 comes in contact with the bottom plate a temperature drop occurs at the interface. After a short period the temperature at the interface starts to increase. At the outside of the bottom plate the melting temperature of 1540 °C is not reached within 4000 s.

Figure 4.3 gives for case PC1 the axial temperature distribution through the bottom plate and the melt at the centre line of the vessel. In this figure the outside of the bottom plate is situated at the horizontal coordinate 0 mm, the transition at horizontal coordinate 100 mm and the top of the melt at horizontal coordinate 250 mm. Figure 4.3 shows that in the oxidic melt an axial temperature gradient is present which becomes stationary within 2000 s. The temperature at the outside of the bottom plate increases with time but at t = 3000 s the temperature distribution is almost stationary.

The development of the crust formation and of the melting of the bottom plate is presented in Figure 4.4 for case PC1. This Figure gives the thickness of the crust at the centre line of the vessel and at a radial distance r = 178 mm. At the same locations the depth of the pool with molten steel is given. As a result of the temperature drop at t = 0 s a layer of solidified Al_2O_3 will be built up at the interface. After a short period the temperature at the interface starts increasing and the crust starts to melt. After 1000 s the temperature at the interface exceeds the melting temperature of steel and the bottom plate starts melting as can be seen in Figure 4.4.

For PC2 - PC5 similar xy-graphs are presented in Figure 4.5 - Figure 4.16.

A comparison of the results is made in Figure 4.17 and in Table 4.1. In Figure 4.17 the temperature history is depicted respectively at the interface and the outside of the bottom plate at the centre line of the vessel (r = 0).

In Table 4.1 the formation of the crust in the melt and the formation of the pool with molten material in the bottom plate is compared. In this table the following is summarized:

- t_m : the point in time at which the melting process in the bottom plate starts;
- d_m : the depth of the pool with molten material at r = 0 for t = 4000 s;
- d_c : the maximum thickness of the crust at r = 0.

Table 4.1 *Data concerning formation of crust and pool with molten material.*

Case	t_m [s]	d_m [mm]	d_c [mm]
PC1	1020	43.5	14.3
PC2	944	43.5	12.0
PC3	1020	43.5	14.3
PC4	1440	38.4	26.2
PC5	348	33.9	3.9

The parameter p in the power law for the conductivity multiplier is varied in the analyses PC1, PC2 and PC3 (p = 3, 1, 5 respectively). Comparing the results for these analyses it appears that the discrepancies in the temperature fields are very small and as a result the crust formation in the oxidic melt and the melting process in the bottom plate are in good agreement. So, the influence on the temperature distribution of the parameter p in the multiplier function is small.

For reasons of comparison also results are presented for the case where the heat conductivity is not modified for convection (PC4; $\lambda^* = \lambda$) and for the case with a jump in the heat conductivity (PC5; $\lambda^* = 10000$ W m^{-1} °C^{-1} for $T > 2050$ °C). Comparing the results of PC4 and PC1 it appears that the temperature gradient is much higher for PC4. At the interface the temperatures for PC4 are smaller. As a consequence the maximum thickness of the crust is higher and the melting process of the bottom plate will start later in time.
Comparing the results of PC5 and PC1 it appears that no temperature gradient is present for PC5 and the temperature at the interface is initially much higher. So only a very thin crust can be built up, while the melting process in the bottom plate starts at 348 s.

HL series with temperature independent heat links
For the nodal points indicated in Figure 3.2 the temperature as function of time is depicted in Figure 4.18 and 4.25 respectively for case HL1 and case HL4. Figure 4.19 and 4.26 give the temperature distribution through the bottom plate and the melt at the centre line of the vessel respectively for case HL1 and case HL4. The crust formation and the melting of the bottom plate are depicted in Figure 4.20 and 4.27 for case HL1 and case HL4.

For the cases HL2 and HL3 qualitative similar results were obtained. For this reason a limited number of graphs is included in this report. In Figure 4.21 and 4.23 the temperature as function of time for the nodal points at the centre line of the vessel is given for case HL3 and case HL4. The formation of the crust and the pool at the centre line is depicted in the Figure 4.22 and 4.24.

The results of this series are compared among each other and with case PC1 in Figure 4.28, which depicts the temperature history at the interface and at the outside of the bottom plate for r = 0 mm. An increase in the heat resistance at the interface is modelled by decreasing the heat transfer coefficient in the heat link elements. For lower heat transfer coefficients the temperature in the oxidic material will be higher while the temperature in the bottom plate will be lower at the interface. So in case of high heat resistance at the interface the oxidic crust will be thin. At the centre line the crust will be molten again in short time.

Due to the lower temperatures in the bottom plate the melting process will start later and the pool depth will be smaller.

At the outside of the bottom plate the influence of the heat resistance on the temperatures is only small.

HL series with temperature dependent heat links
For these series the temperature history in the nodes at the centre line of the vessel are depicted in the Figures 4.29, 4.31, 4.33, 4.35 and 4.37. The formation of crust / pool is shown in the Figures 4.30, 4.32, 4.34, 4.36 and 4.38.

To compare the results obtained with the temperature dependent heat links with the results obtained with the temperature independent heat links the results for case HLx and case HLy are shown also in the figures for case HLxy. Immediately after the molten oxidic melt comes into contact with the bottom plate a crust will be built up and the heat resistance is high at the interface. It appears that the temperature distribution is identical to the one obtained with a constant low heat transfer coefficient. The temperatures in the crust increases and the crust will melt completely at the centre line and the heat resistance will drop to low value. Due to this drop some numerical problems arise in the analyses with the largest difference between the low and the high value in heat resistance (HL13 and HL24). As can be seen in the figures 4.31 and 4.35 the calculated temperature shows an oscillating behaviour after remelting of the crust. These oscillations can be reduced by choosing a much smaller time increment. After a transition period the temperature distribution becomes identical to the one obtained with a constant high heat transfer coefficient. The length of the transition period depends on the low and high value of the heat transfer coefficient.

The crust formation for the temperature dependent heat transfer coefficient (analysis HLxy) and the corresponding low constant heat transfer coefficient (analysis HLx) is similar. The formation of a pool of molten material in the bottom plate is similar for the temperature dependent heat transfer coefficient and the corresponding high constant heat transfer coefficient (analysis HLy).

Discussion
The results presented show that it is possible to model crust formation at the interface of an oxidic melt and a steel bottom. A modified heat transfer coefficient was defined to simulate the heat transfer by convection in the liquid corium. The heat resistance at the interface was simulated by means of heat link elements. The validation of this model is not part of this report but should be done in future considering experimental results. For this purpose there is a need for temperature profiles through the thickness of the test section as well as temperature data in the melt. This can only be realised in an experiment where temperature evolution and mechanical degradation develop without dynamic effects. Practically, this means an experiment without penetrations. However, useful data might also be obtained, in case of plugging of the melt in a tube.

5. SUMMARY AND CONCLUSIONS

To study the possibilities of modelling crust formation at the interface of an oxidic melt and a steel bottom plate with a solid element model a modified heat transfer coefficient was defined to simulate the heat transfer by convection in the liquid corium. Above the melting temperature of Al_2O_3 (2050 °C) the true conductivity of the oxidic material is increased by a temperature dependent conductivity multiplier. In this study for this multiplier a power law of order p was chosen. With this modified conductivity model a number of FE-analyses was made for p = 1, 3, and 5. For reasons of comparison an additional analysis was made without correction for heat transport due to convection (multiplier is equal to 1) and also an analysis was made with a jump in the conductivity as was used in former analyses.
From these analyses it can be concluded that:

- Immediately after the molten corium comes in contact with the steel plate an oxidic crust will be built up and the melting of the bottom plate will initiate later on. So it is possible using a solid model to simulate crust formation taking into account the heat transfer by convection.
- The result of an increased conductivity in the liquid corium is that the crust will be thinner and that the melting process in the bottom plate will initiate earlier.
- The influence of the parameter p in the power law on the calculated temperature field in the corium and in the bottom plate is only very small for values of p in the range 1 - 5.

For an oxidic melt it is expected that the wetting will not be as good as for an iron melt. To determine the influence of heat resistance at the interface of melt and bottom plate a number of FE-analyses were made with so called heat link elements. The heat transfer coefficient has been taken both constant (temperature independent) and dependent on the temperature of the corium.
From these analyses the following conclusion can be drawn.

- The result of increasing the heat resistance at the interface is that the maximum thickness of the crust decreases and that the initiating of the melting process in the bottom plate will be delayed.

To validate the model for crust formation at the interface and to improve the input variables for heat transfer calculations, there is a need for temperature profiles through the thickness of the test section as well as temperature data in the melt. This can only be realised in an experiment where temperature evolution and mechanical degradation develop without dynamic effects. Practically, this means an experiment without penetrations. However, useful data might also be obtained, in case of plugging of the melt in a tube.

REFERENCES

[1] G. Duijvestijn, K. Nakada, Computational analysis of the CORVIS 01/6 experiment, PSI TM-49-95-04, 3 May 1995

[2] MARC Analysis Research Corporation, MARC User's Manuals, Revision K6.1, 1994.

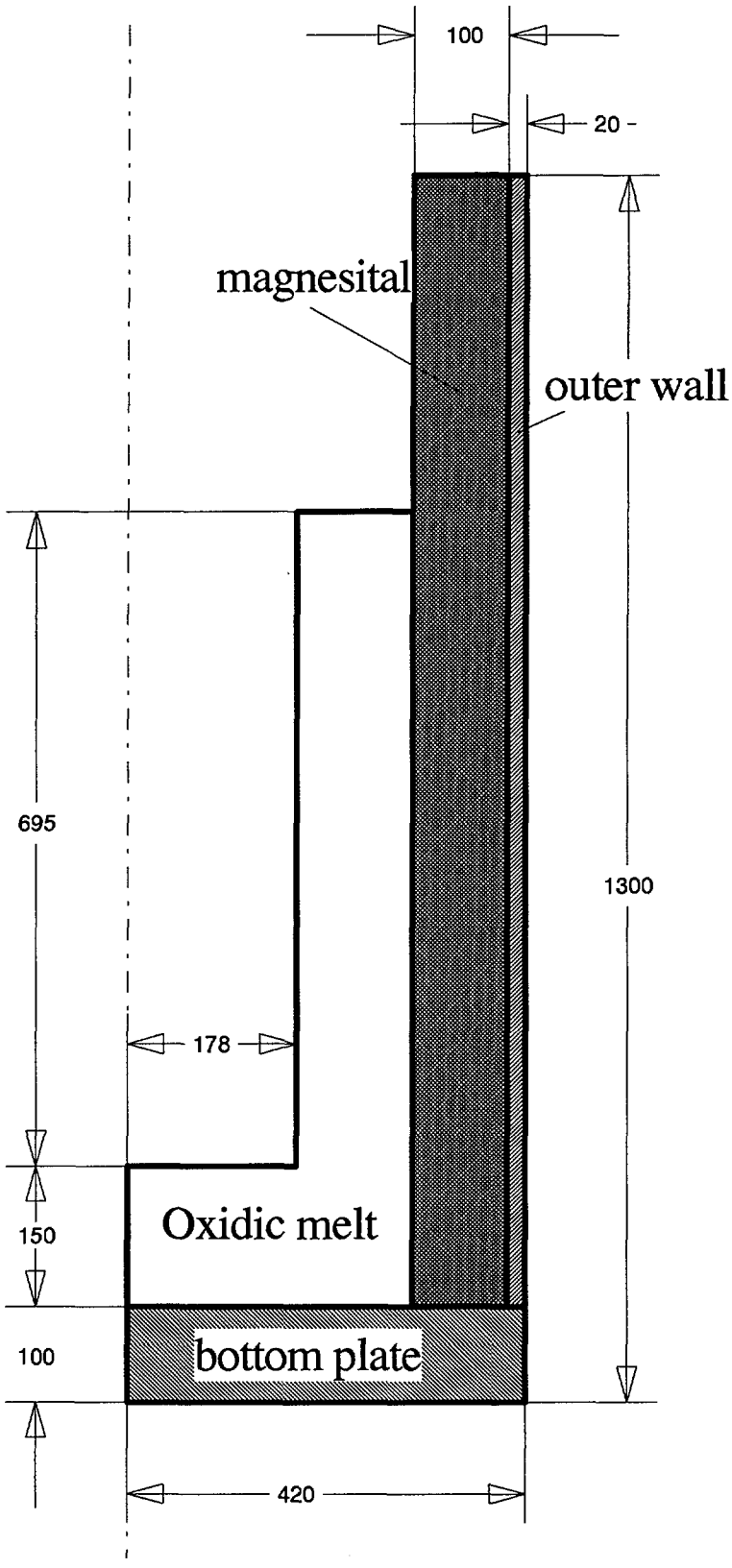

Figure 2.1 *Geometry of the test vessel (dimensions in mm)*

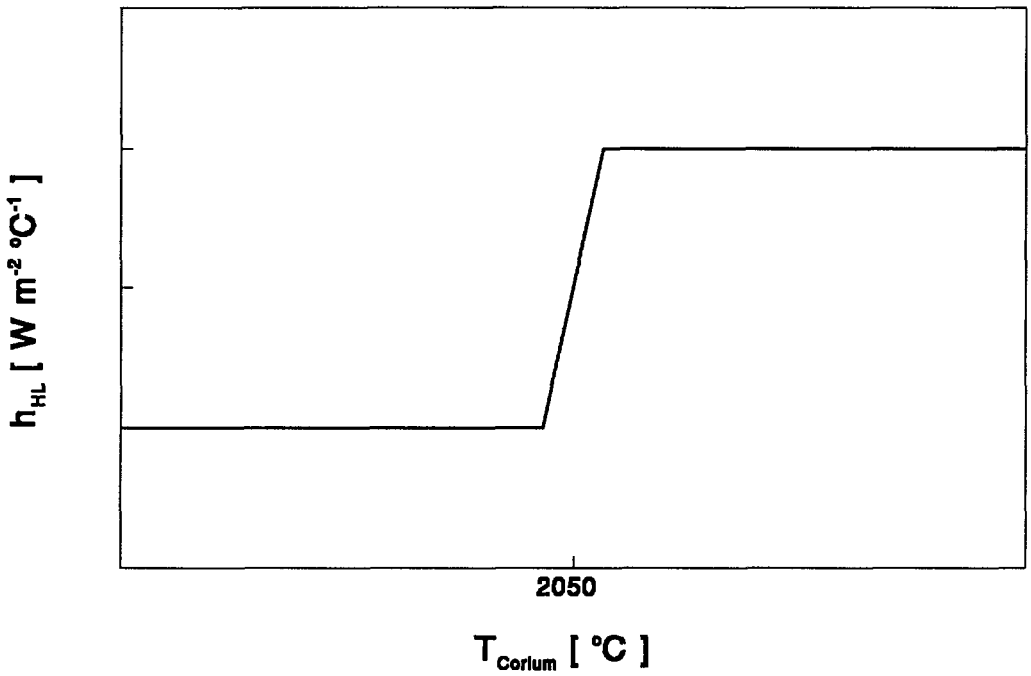

Figure 3.1 *Heat transfer coefficient in heat link elements*

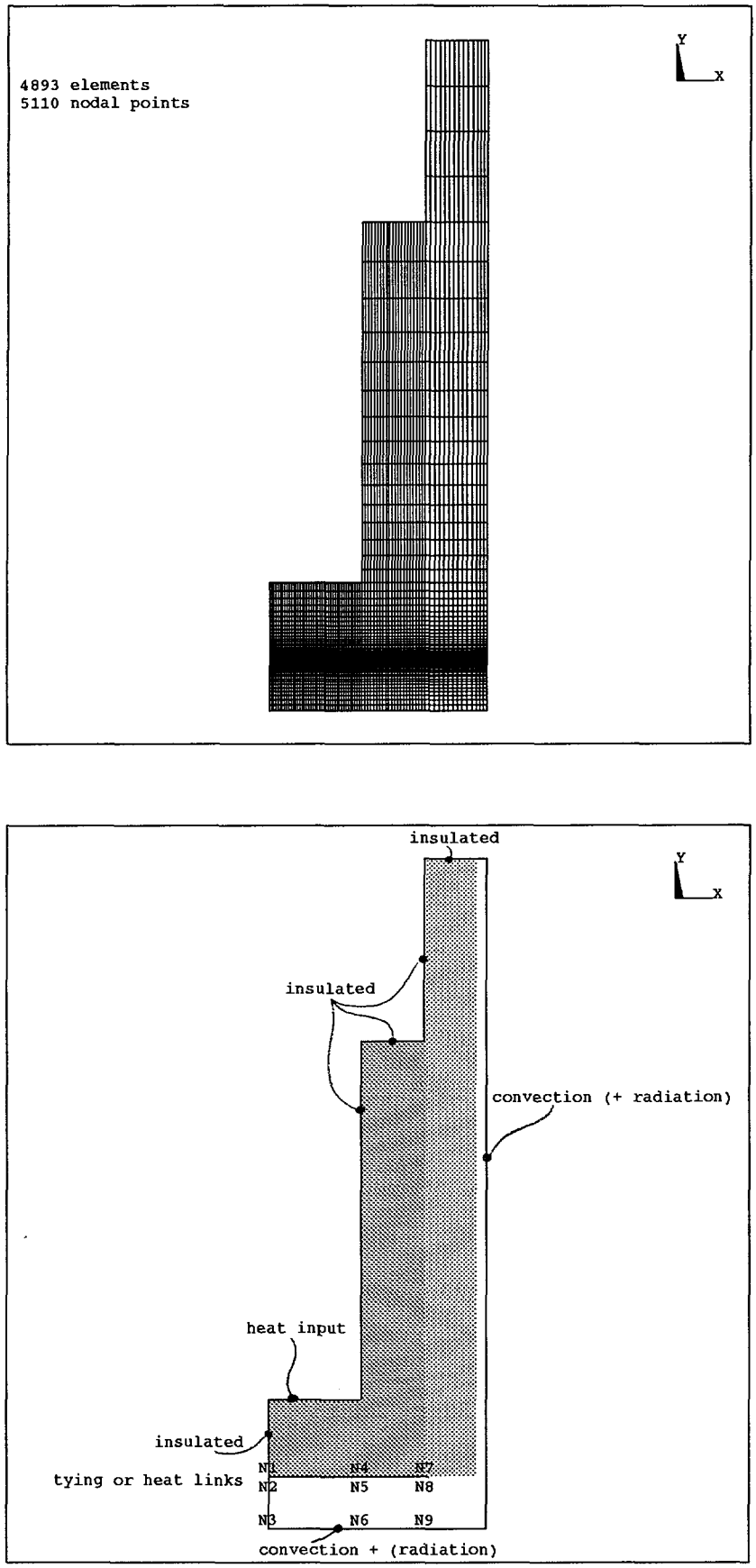

Figure 3.2 *Mesh lay out and boundary conditions*

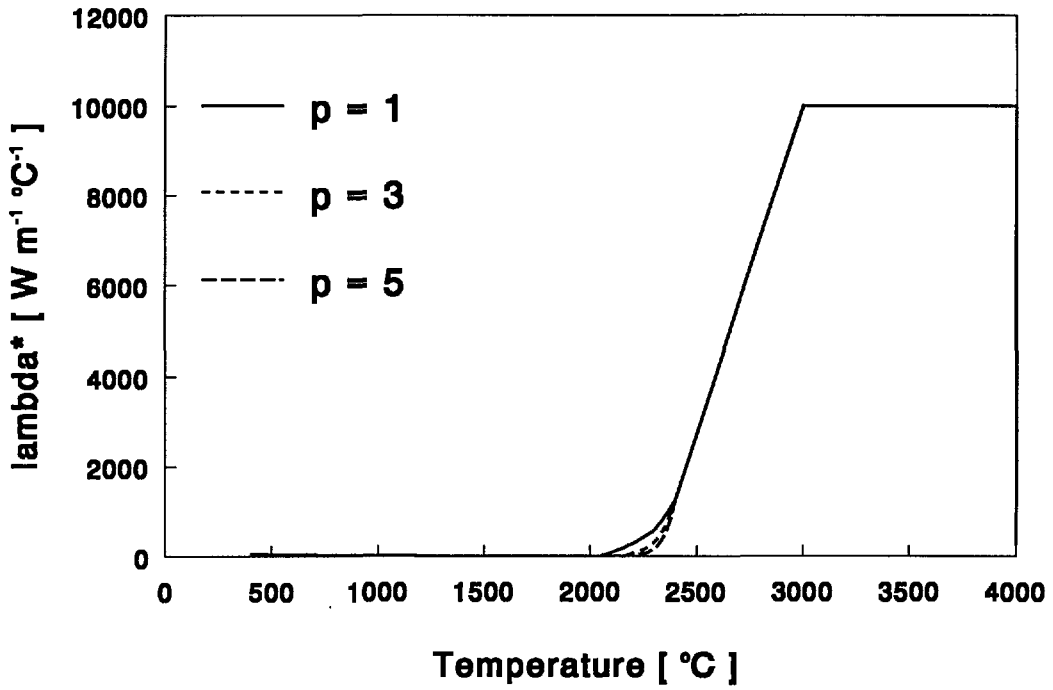

Figure 3.3.a *The modified thermal conductivity of Al_2O_3 as a function of the temperature (0 < T < 4000)*

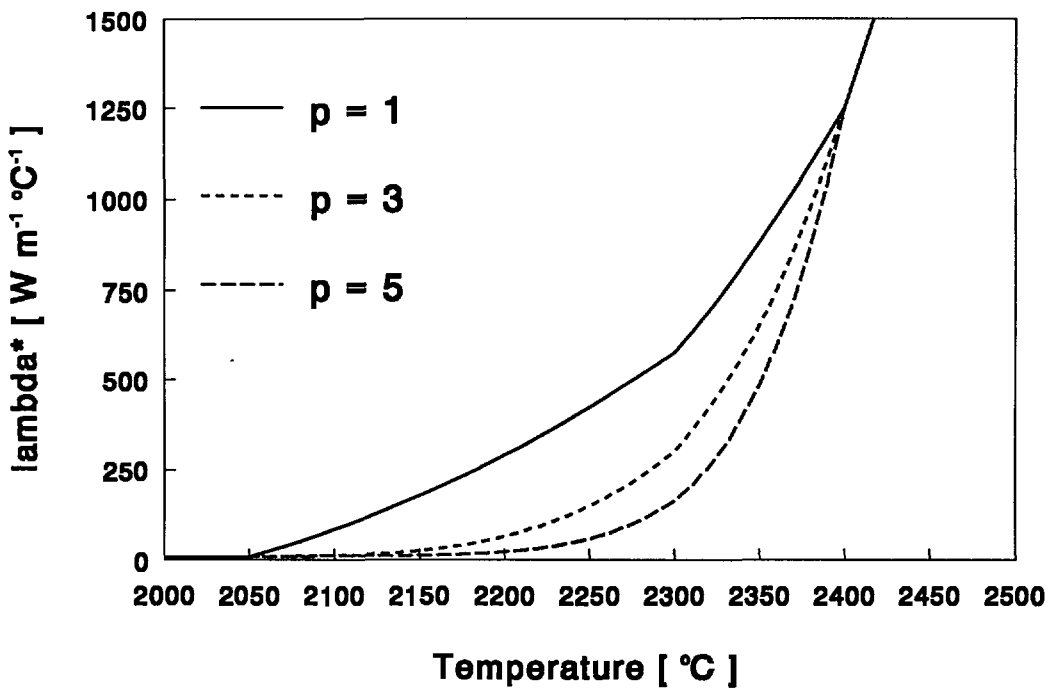

Figure 3.3.b *The modified thermal conductivity of Al_2O_3 as a function of the temperature (2000 < T < 2500)*

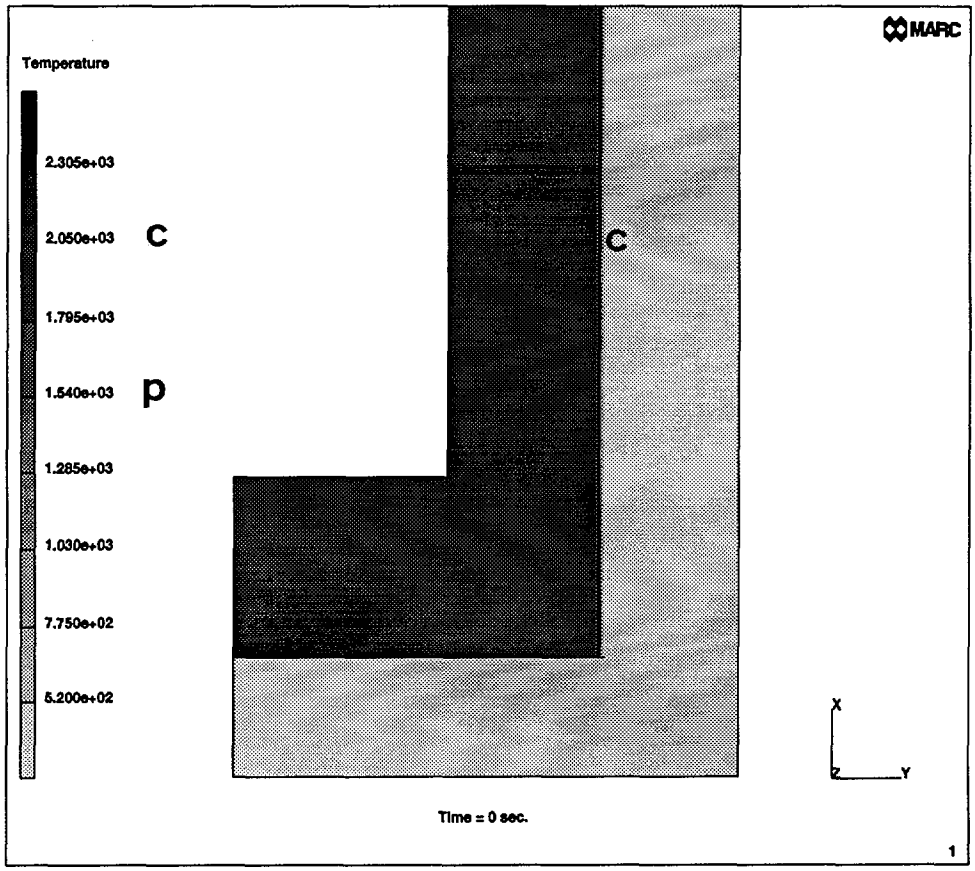

Figure 4.1.a *Temperature field for case PC1 at time t = 0 sec.*

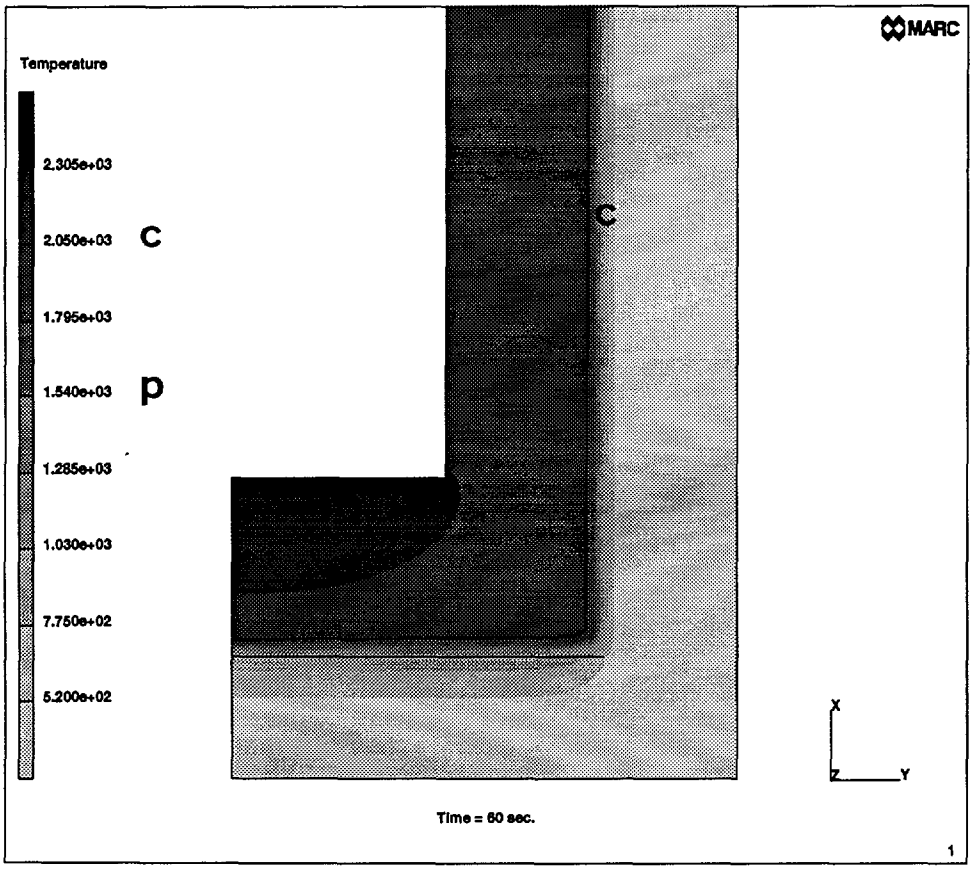

Figure 4.1.b *Temperature field for case PC1 at time t = 60 sec.*

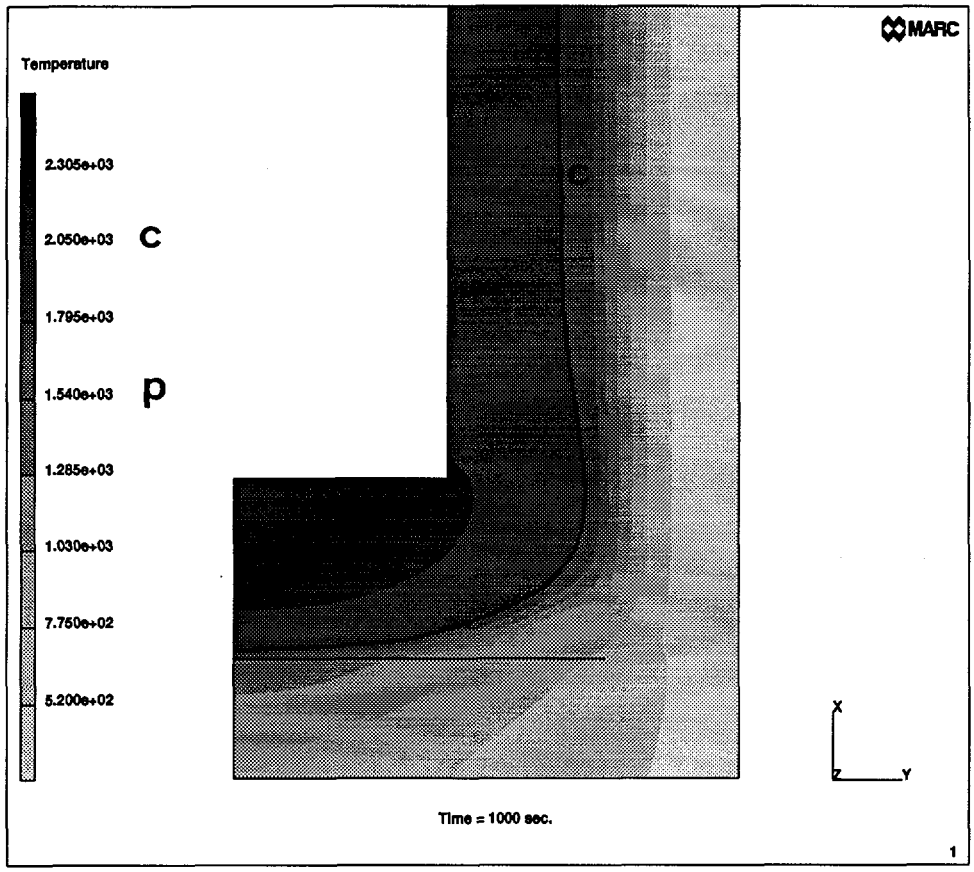

Figure 4.1.c *Temperature field for case PC1 at time t = 1000 sec.*

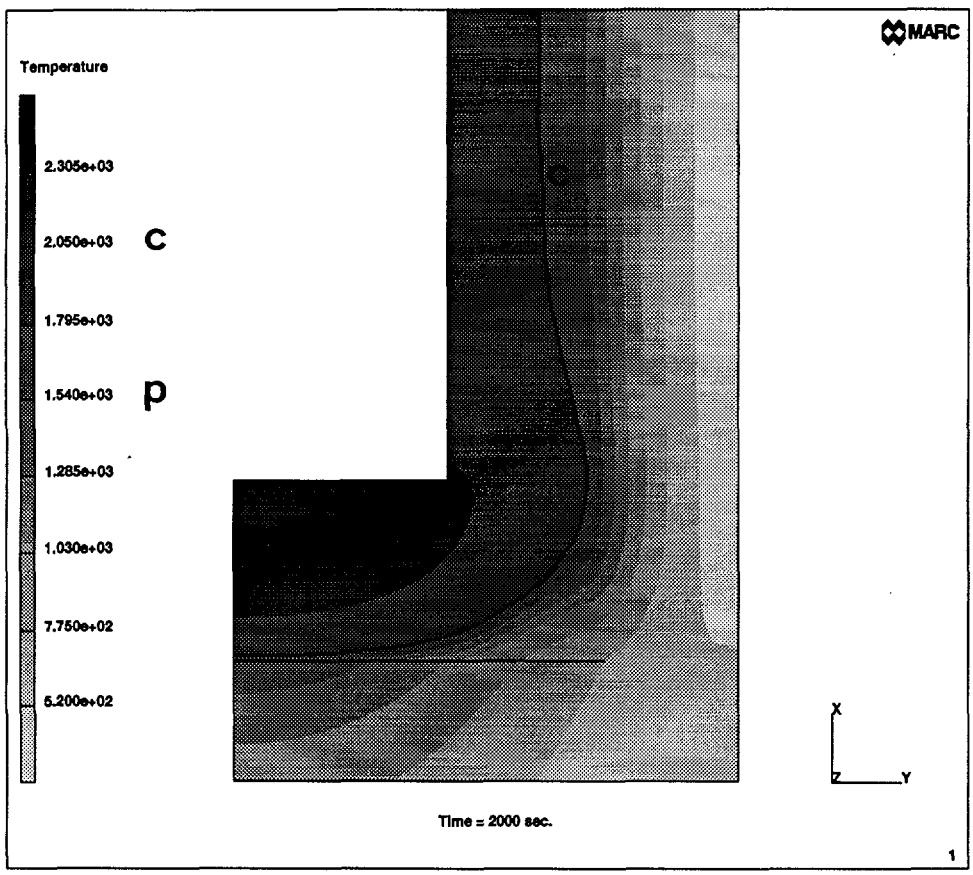

Figure 4.1.d *Temperature field for case PC1 at time t = 2000 sec.*

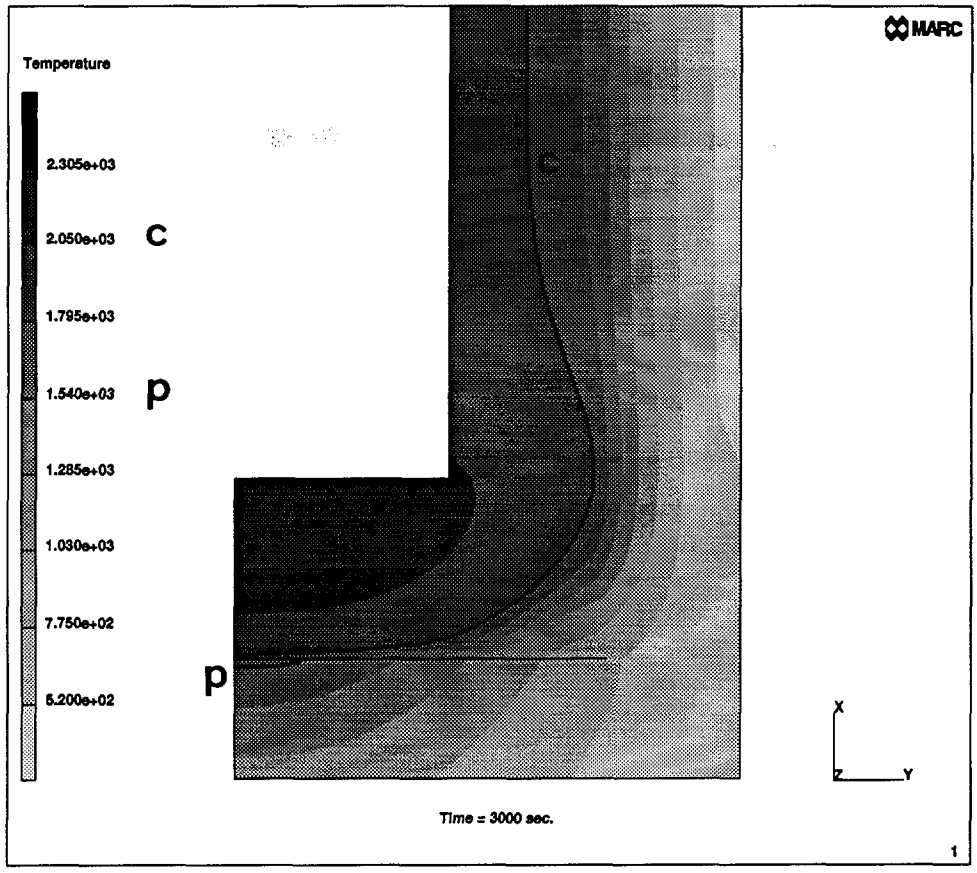

Figure 4.1.e *Temperature field for case PC1 at time t = 3000 sec.*

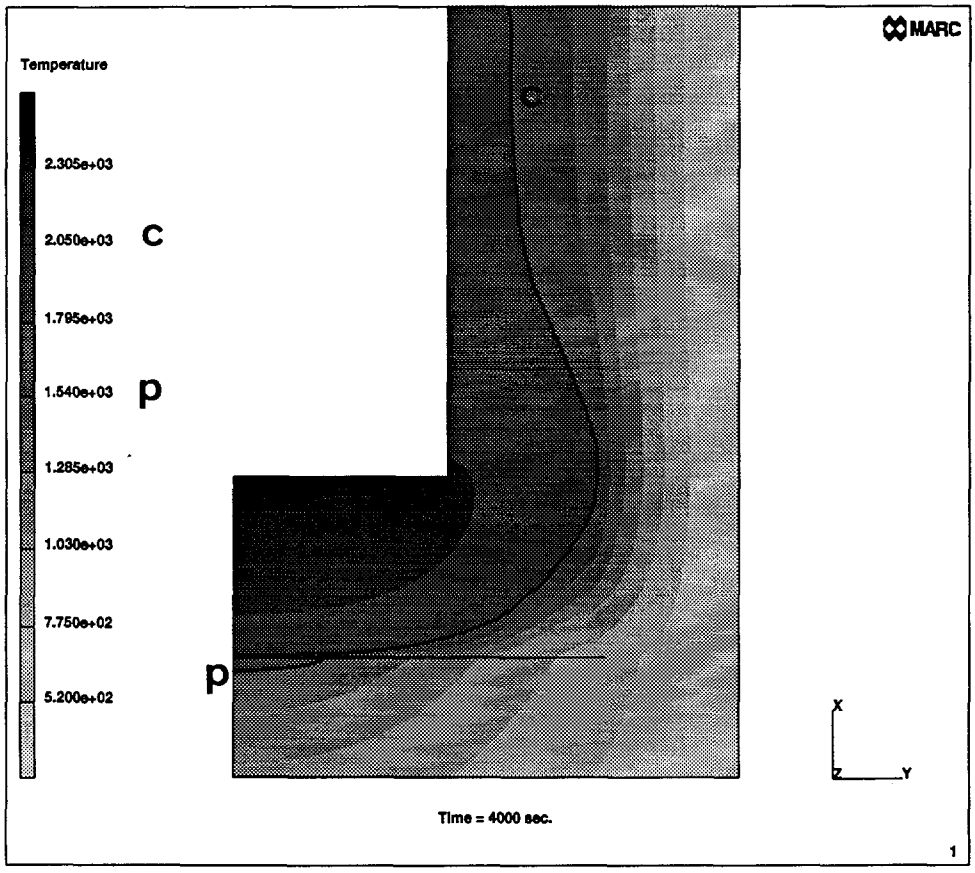

Figure 4.1.f *Temperature field for case PC1 at time t = 4000 sec.*

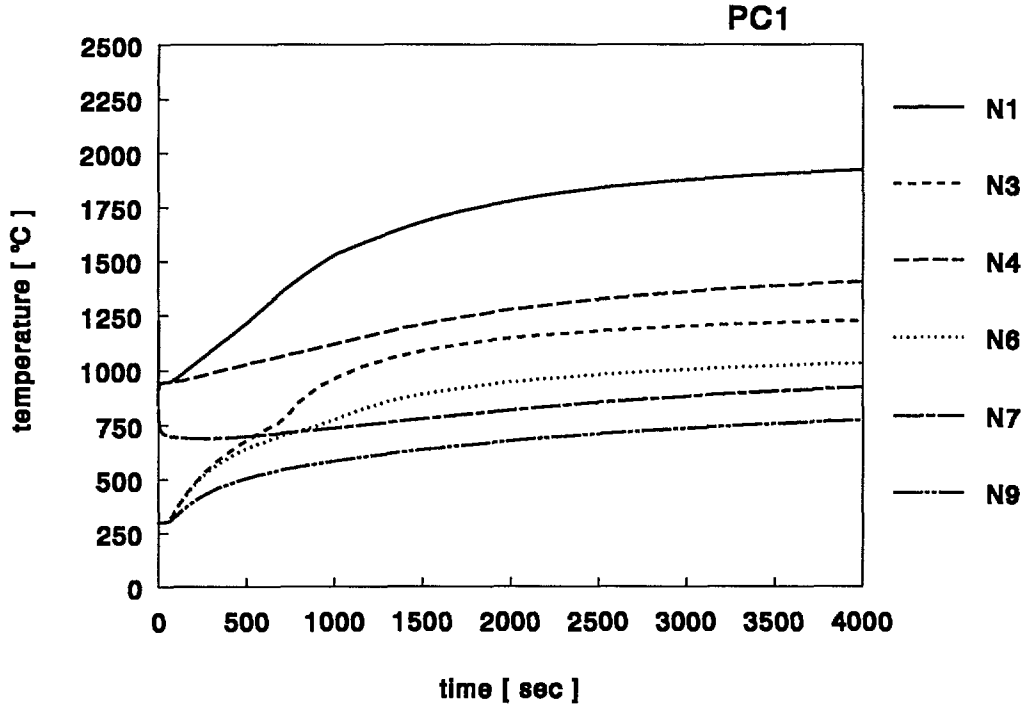

Figure 4.2 *Temperature history for case PC1 at locations depicted in Figure 3.2*

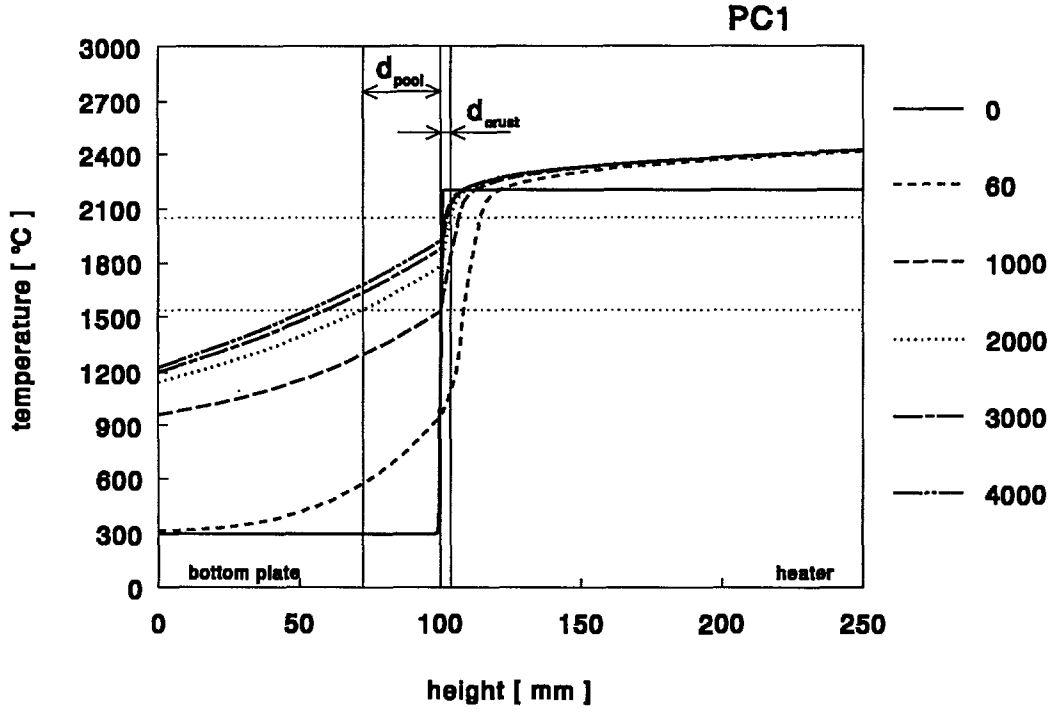

Figure 4.3 *Axial temperature distribution at the center line for case PC1 (the thickness of the crust and the depth of the pool at t = 2000 are indicated)*

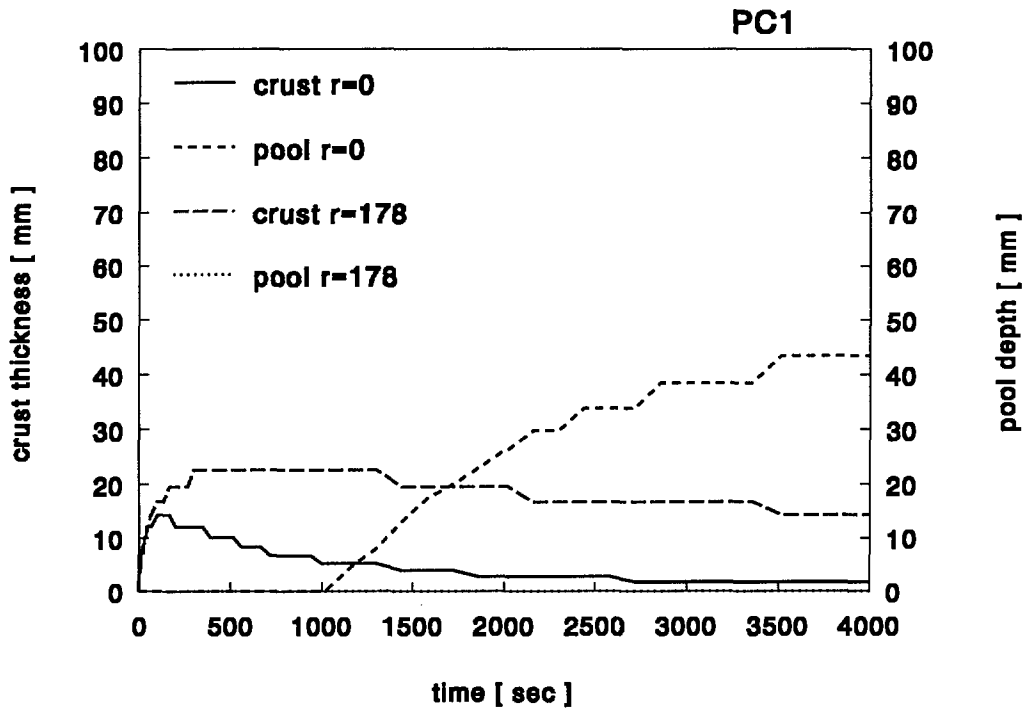

Figure 4.4 *Thickness of the crust and depth of the pool with molten steel at the center line (r = 0 mm) and at a radial distance r = 178 mm for case PC1*

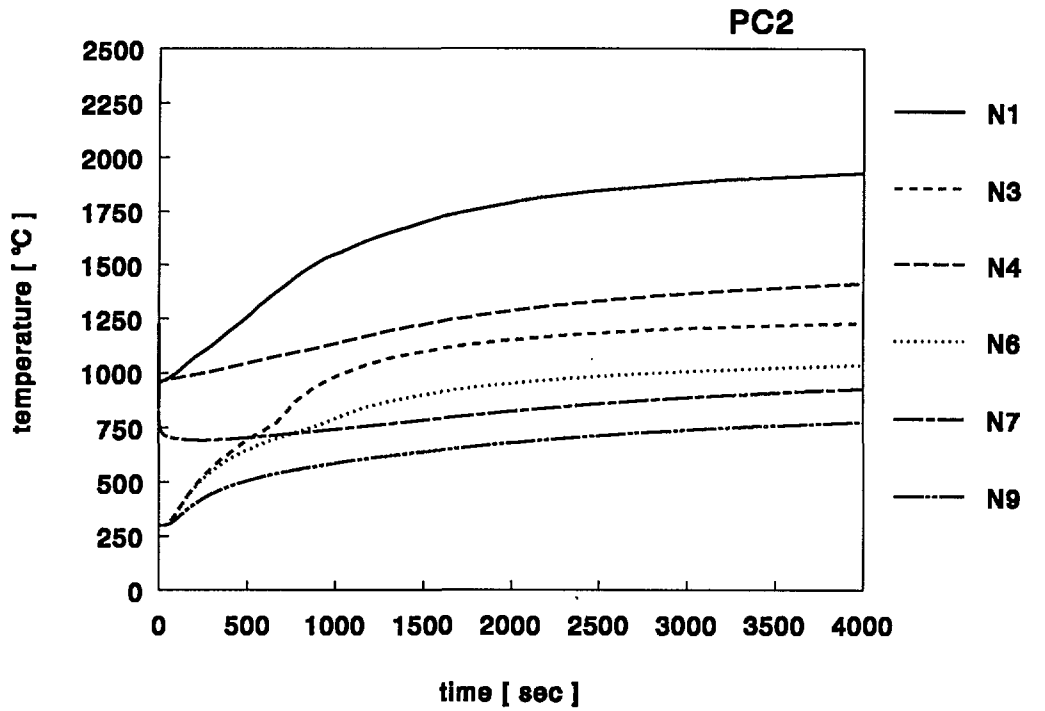

Figure 4.5 *Temperature history for case PC2 at locations depicted in Figure 3.2*

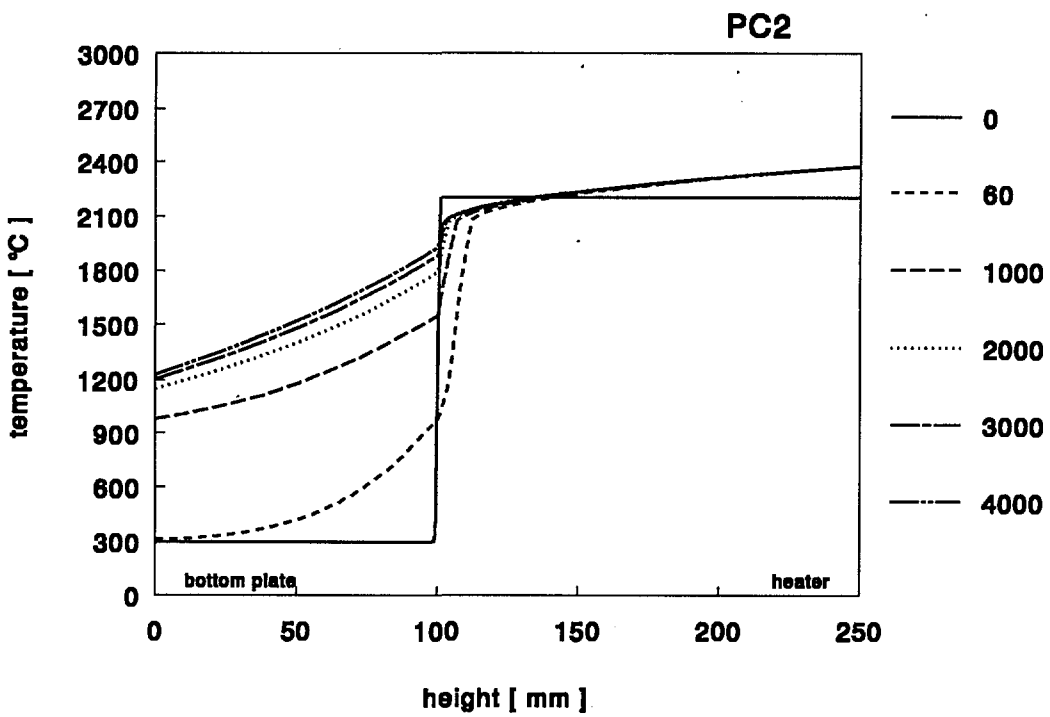

Figure 4.6 *Axial temperature distribution at the center line for case PC2*

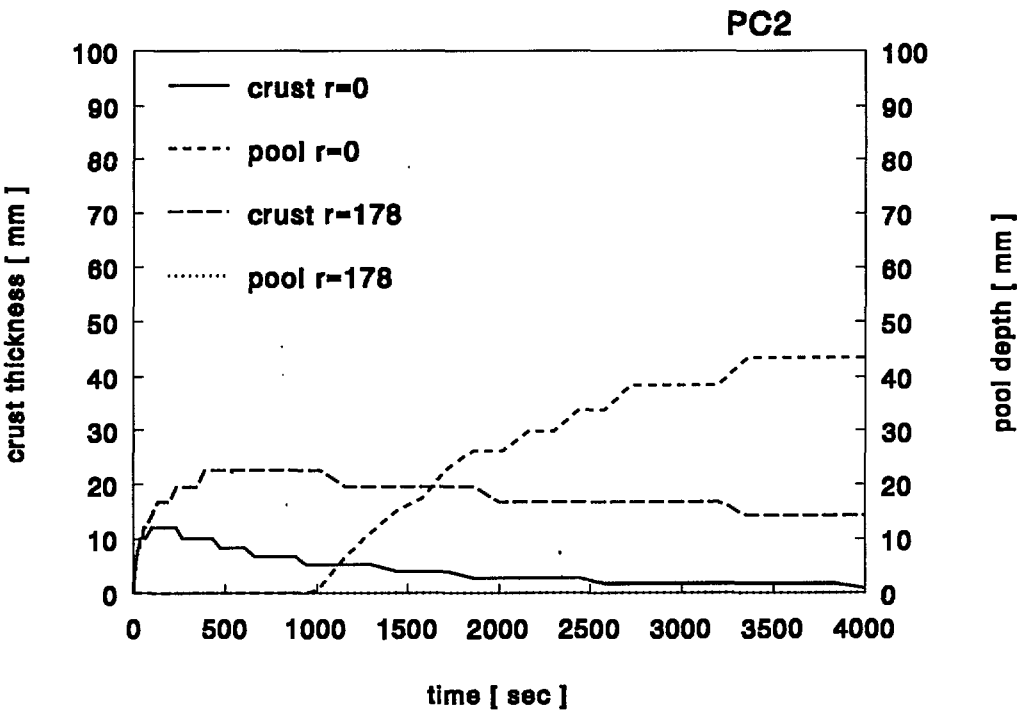

Figure 4.7 *Thickness of the crust and depth of the pool with molten steel at the center line (r = 0 mm) and at a radial distance r = 178 mm for case PC2*

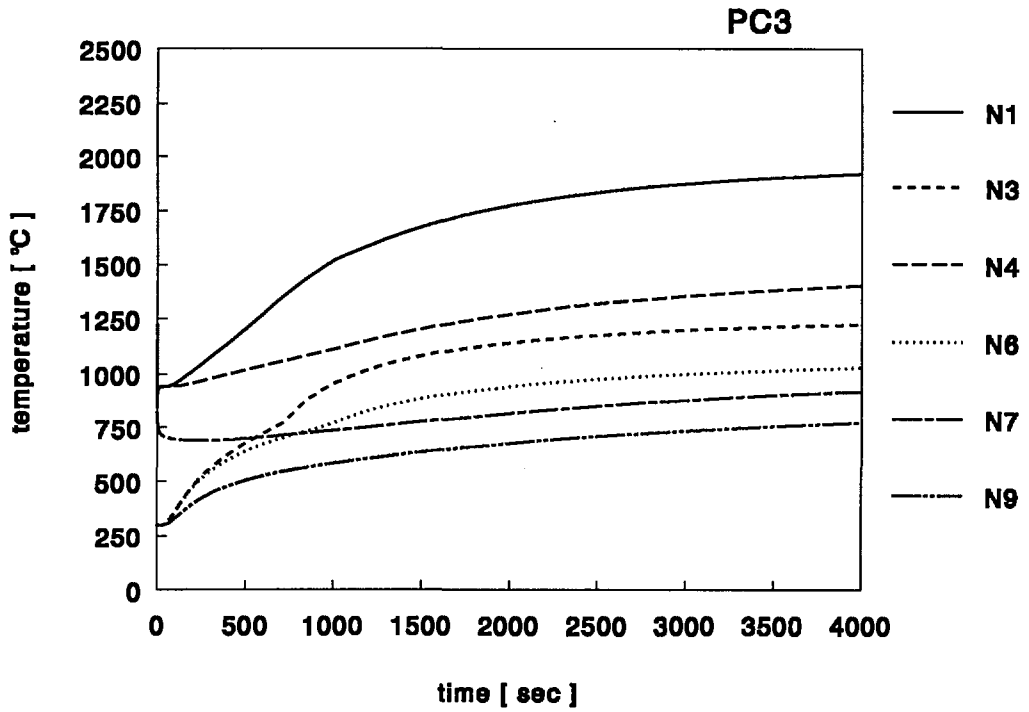

Figure 4.8 *Temperature history for case PC3 at locations depicted in Figure 3.2*

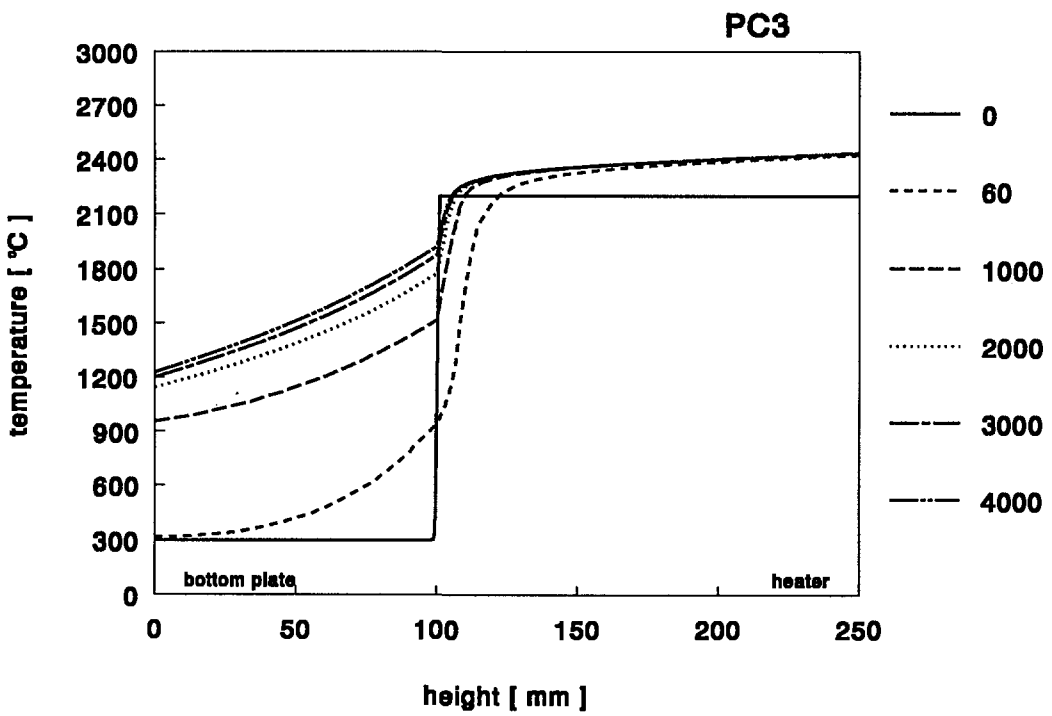

Figure 4.9 *Axial temperature distribution at the center line for case PC3*

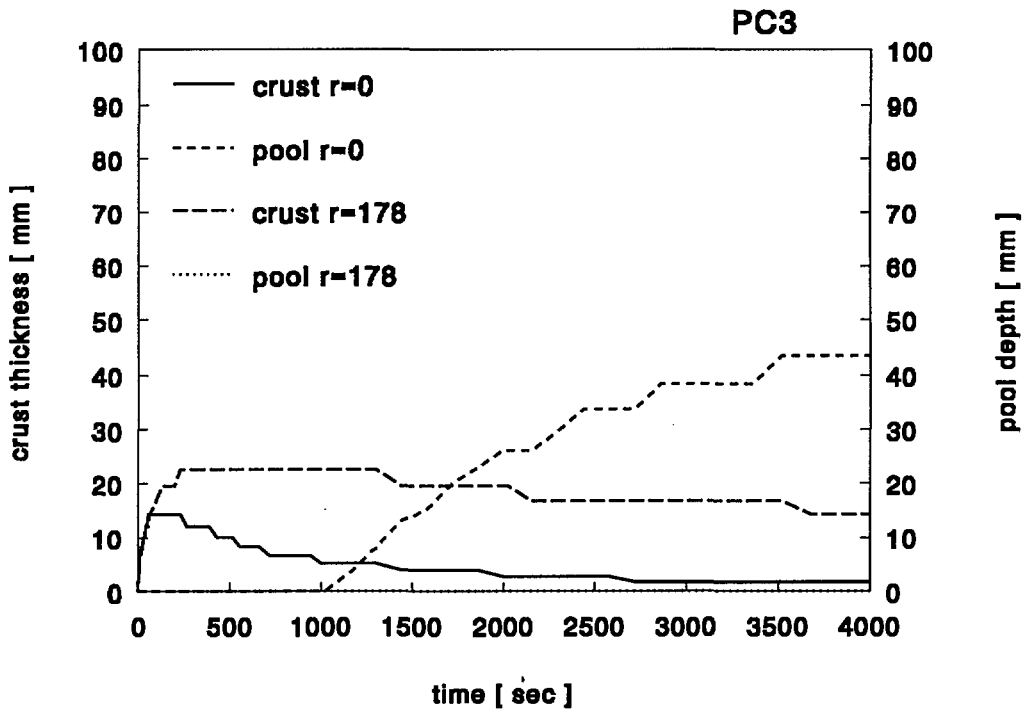

Figure 4.10 *Thickness of the crust and depth of the pool with molten steel at the center line (r = 0 mm) and at a radial distance r = 178 mm for case PC3*

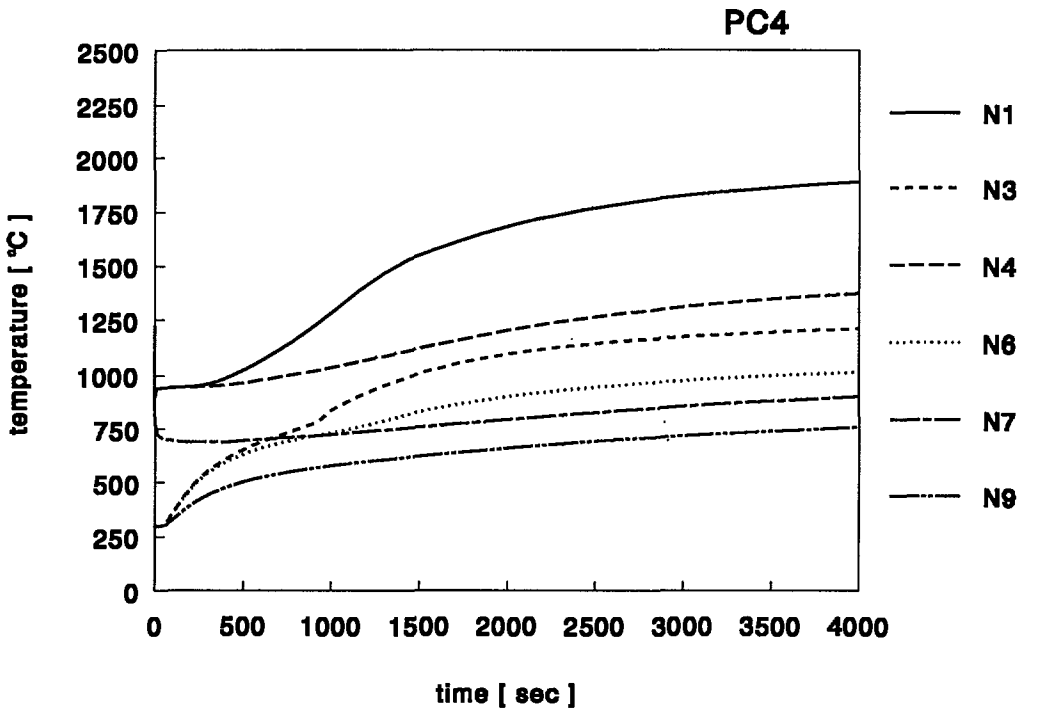

Figure 4.11 *Temperature history for case PC4 at locations depicted in Figure 3.2*

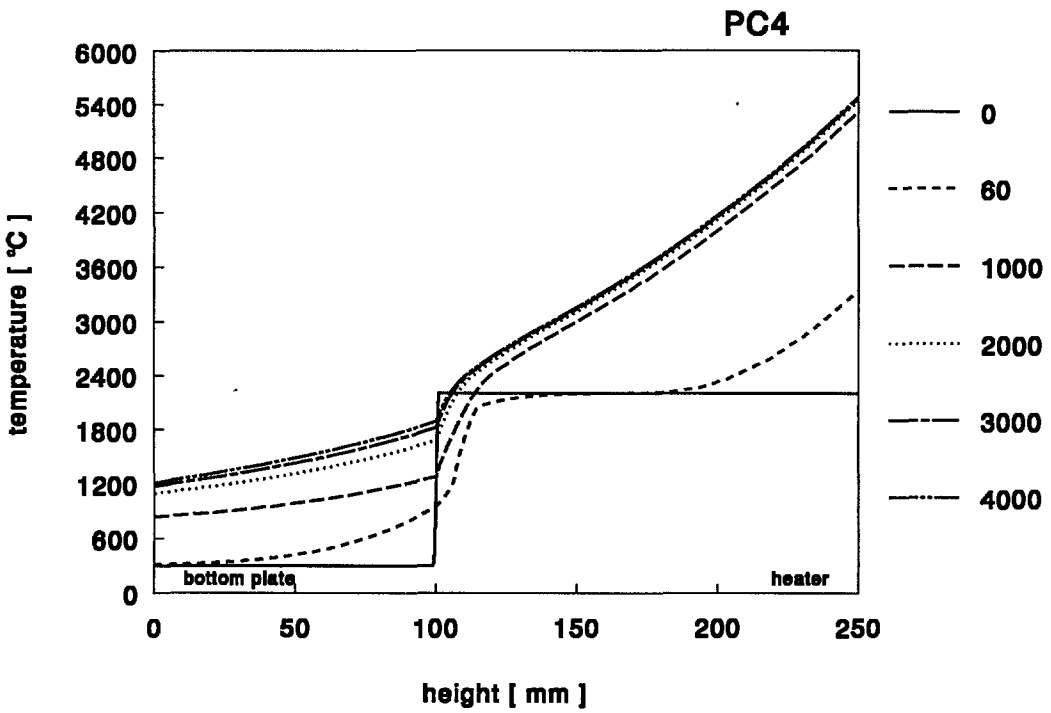

Figure 4.12 *Axial temperature distribution at the center line for case PC4*

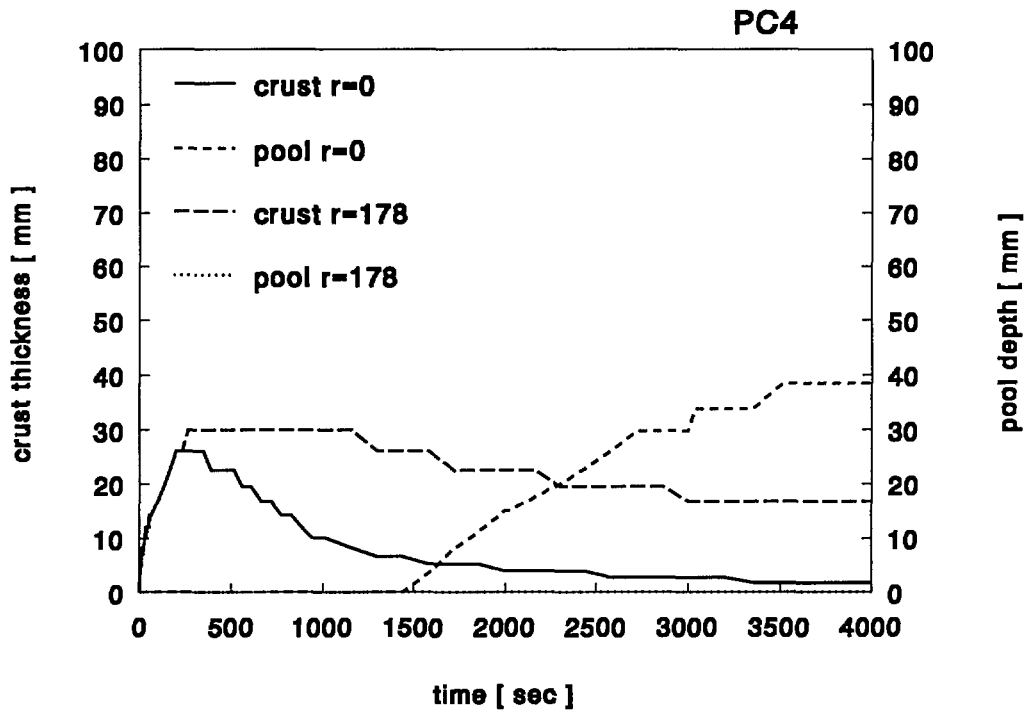

Figure 4.13 *Thickness of the crust and depth of the pool with molten steel at the center line (r = 0 mm) and at a radial distance r = 178 mm for case PC4*

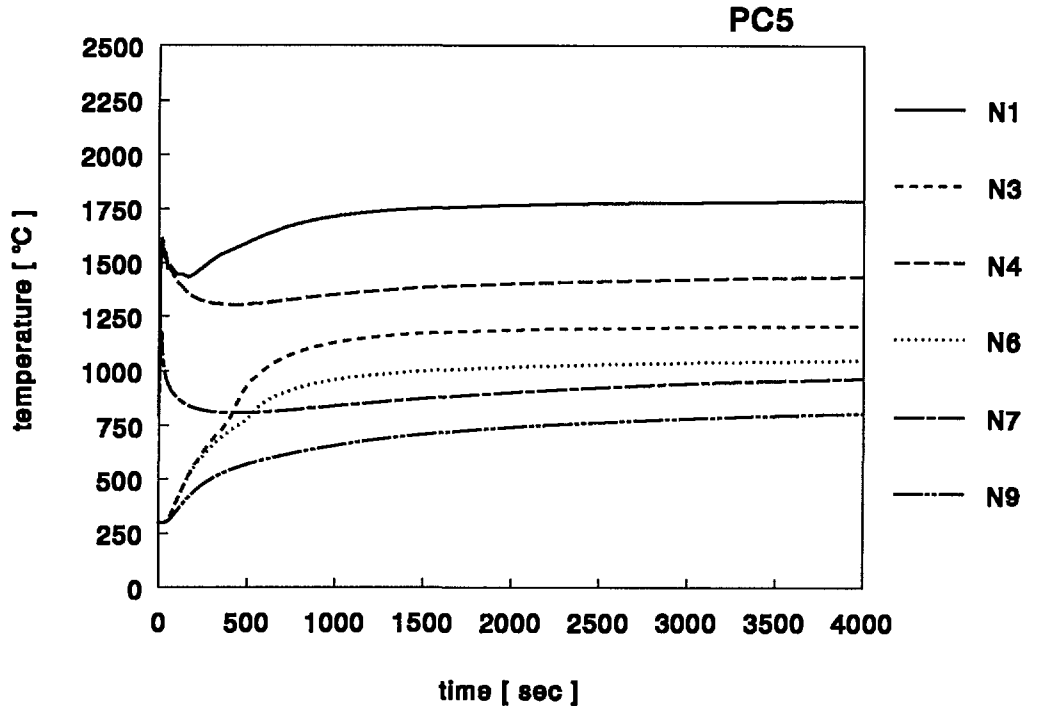

Figure 4.14 *Temperature history for case PC5 at locations depicted in Figure 3.2*

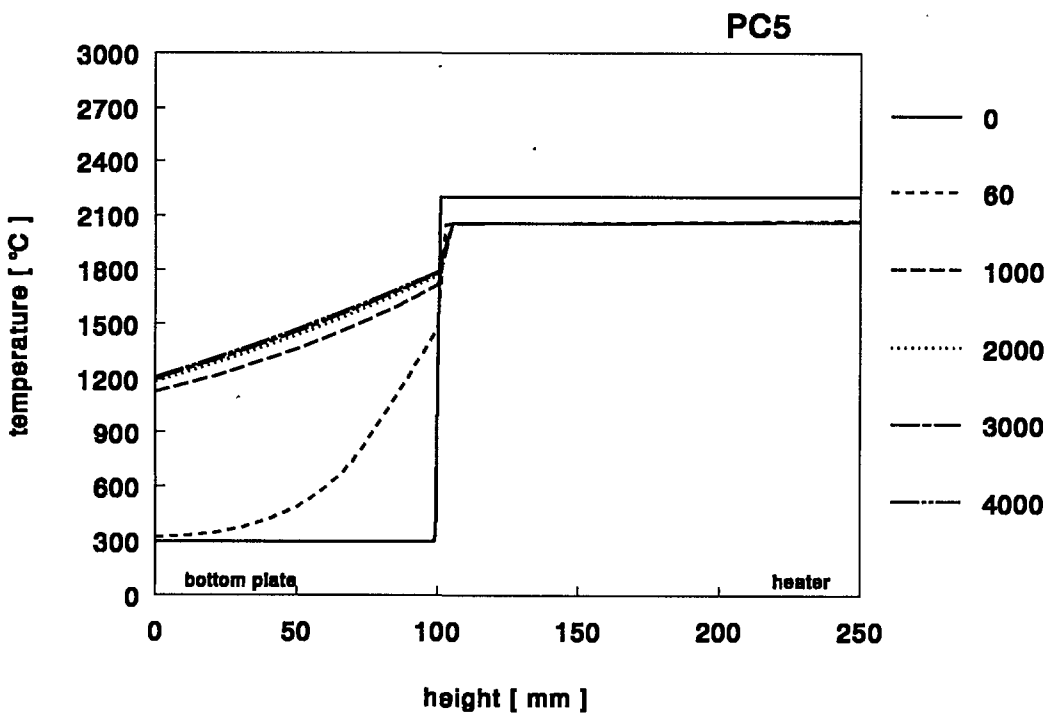

Figure 4.15 *Axial temperature distribution at the center line for case PC5*

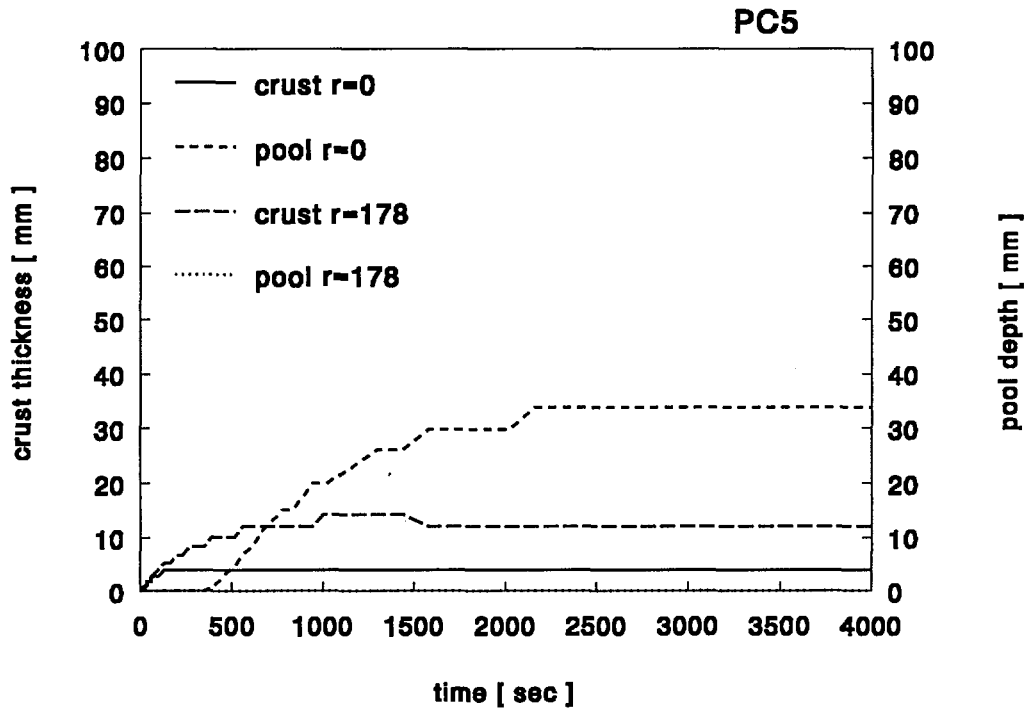

Figure 4.16 *Thickness of the crust and depth of the pool with molten steel at the center line (r = 0 mm) and at a radial distance r = 178 mm for case PC5*

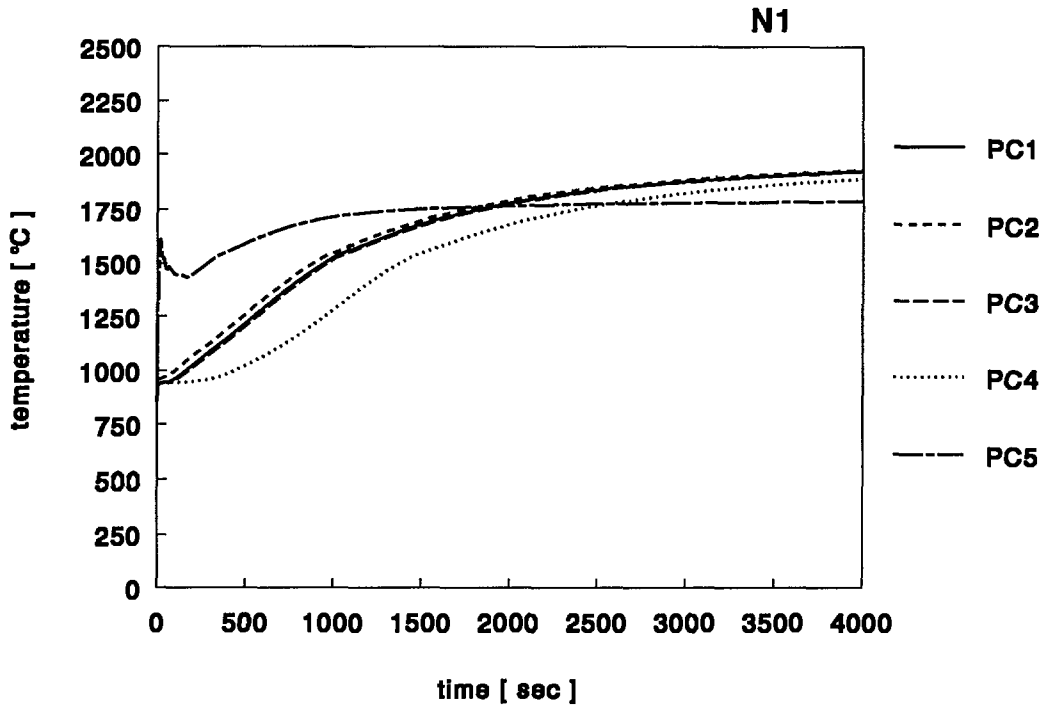

Figure 4.17.a *Temperature history for PC-series at location N1 as depicted in Figure 3.2*

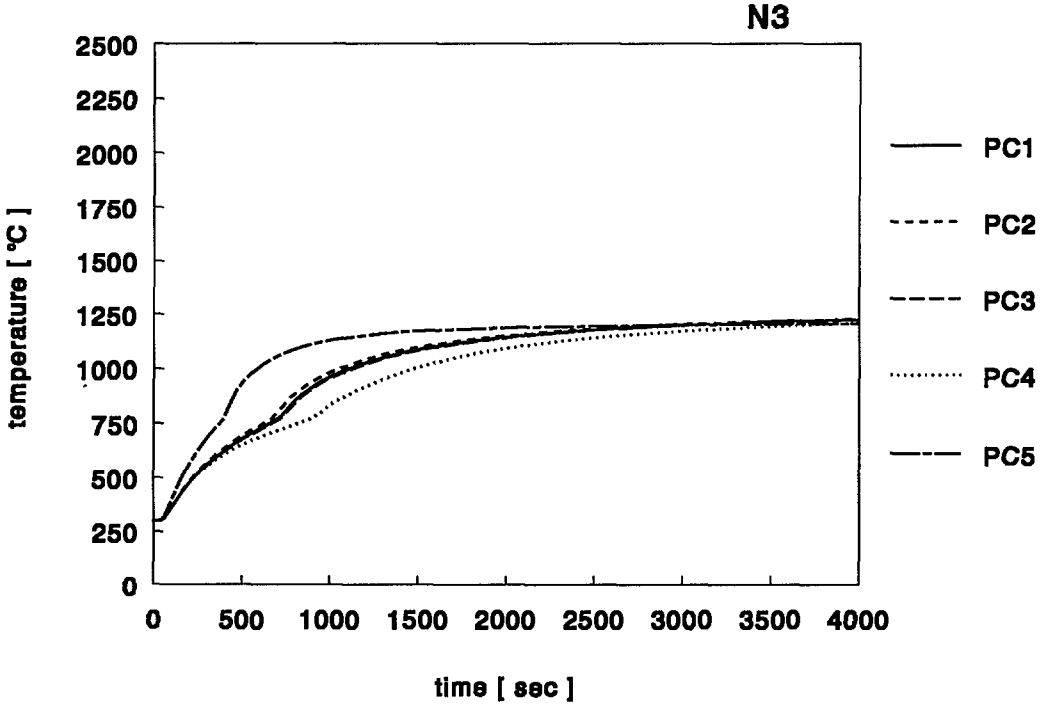

Figure 4.17.b *Temperature history for PC-series at location N3 as depicted in Figure 3.2*

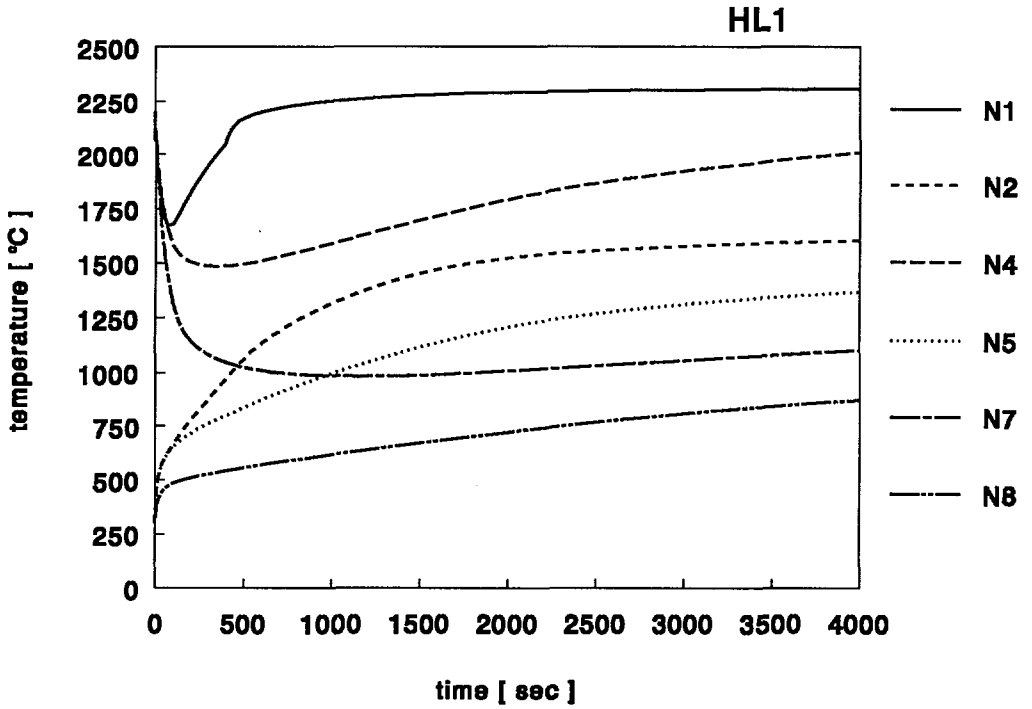

Figure 4.18.a *Temperature history for case HL1 at locations depicted in Figure 3.2*

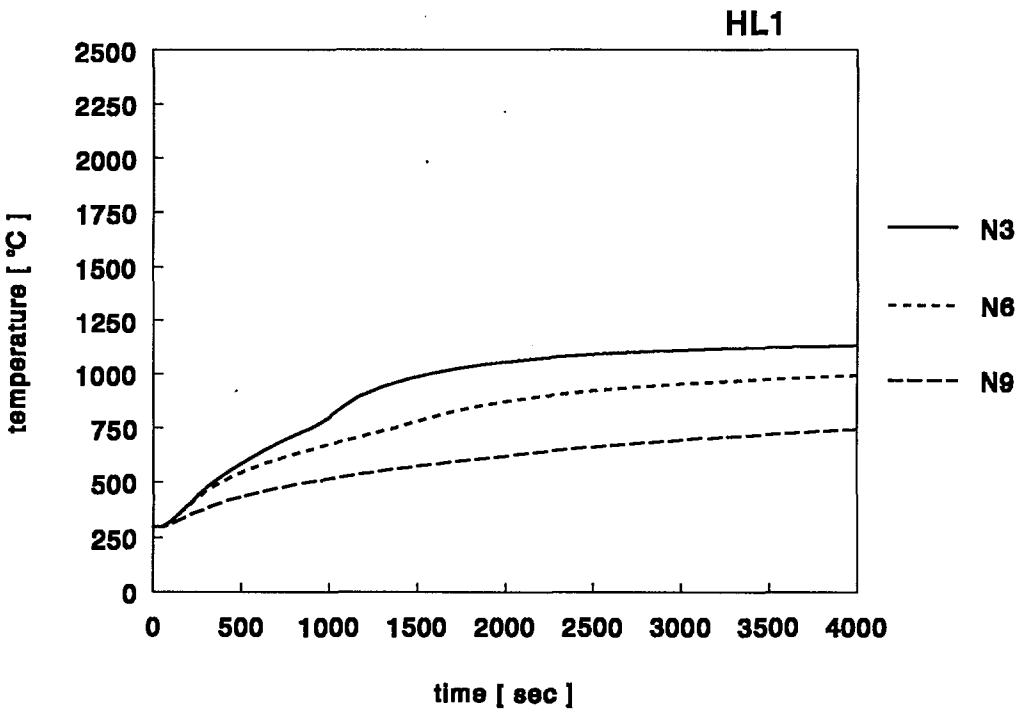

Figure 4.18.b *Temperature history for case HL1 at locations depicted in Figure 3.2*

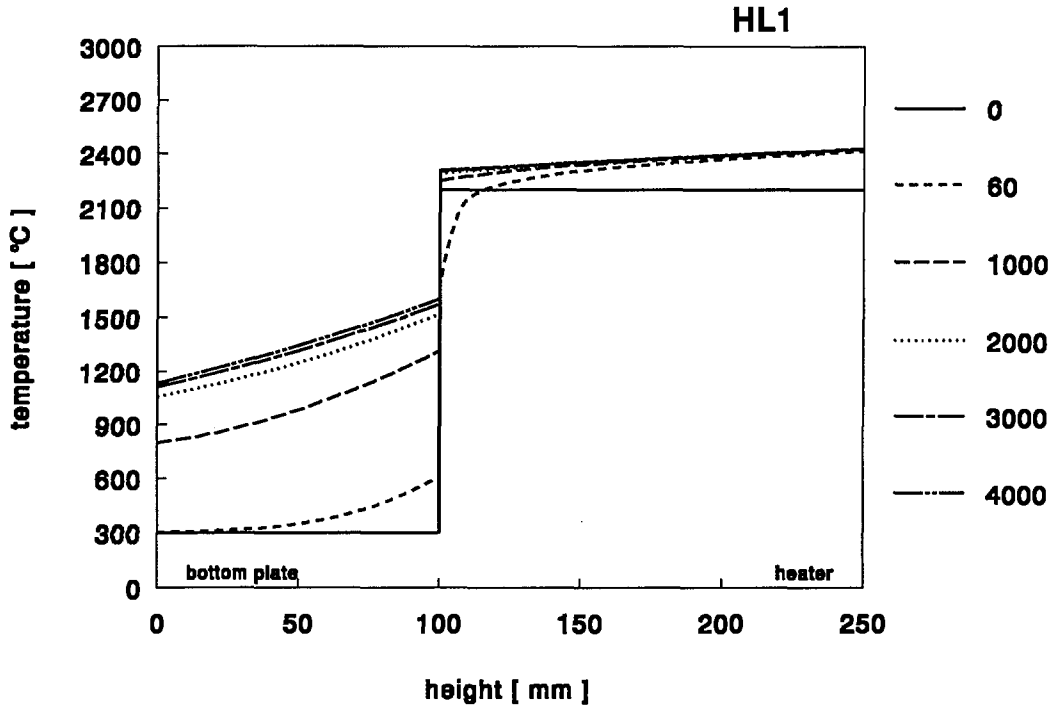

Figure 4.19 *Axial temperature distribution at the center line for case HL1*

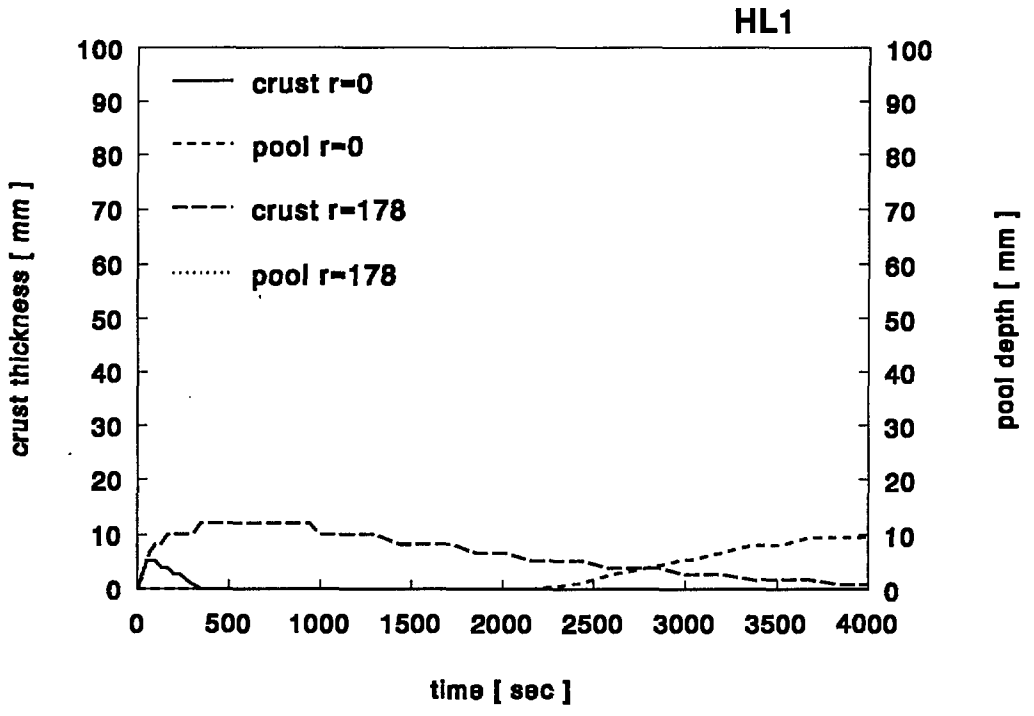

Figure 4.20 *Thickness of the crust and depth of the pool with molten steel at the center line (r = 0 mm) and at a radial distance r = 178 mm for case HL1*

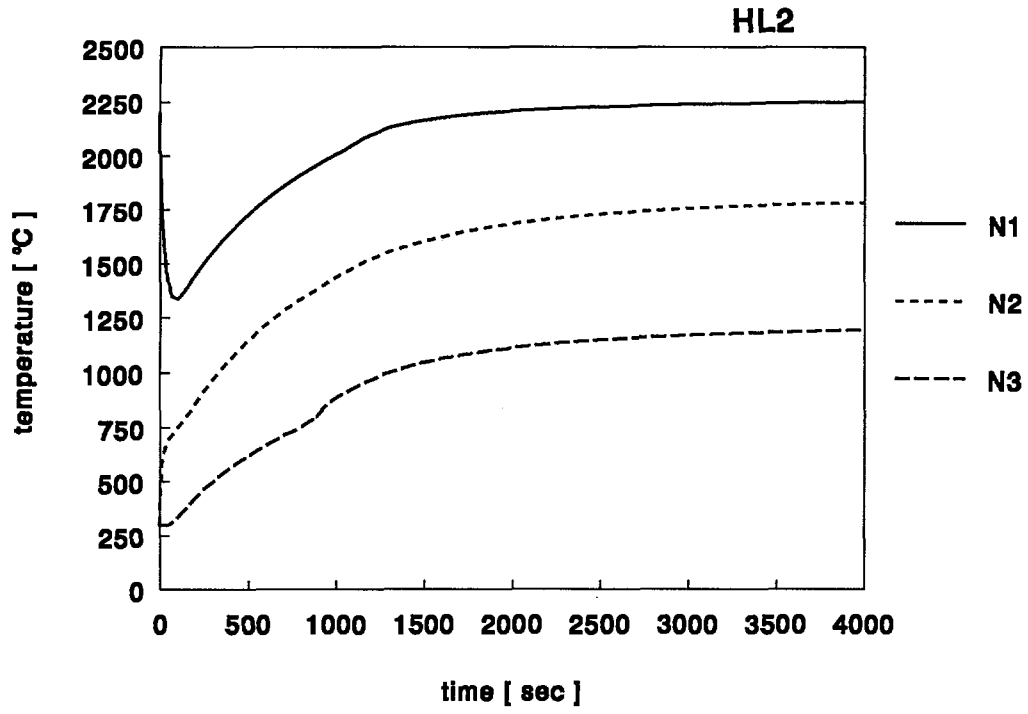

Figure 4.21 *Temperature history for case HL2 at nodes N1, N2 and N3 as depicted in Figure 3.2*

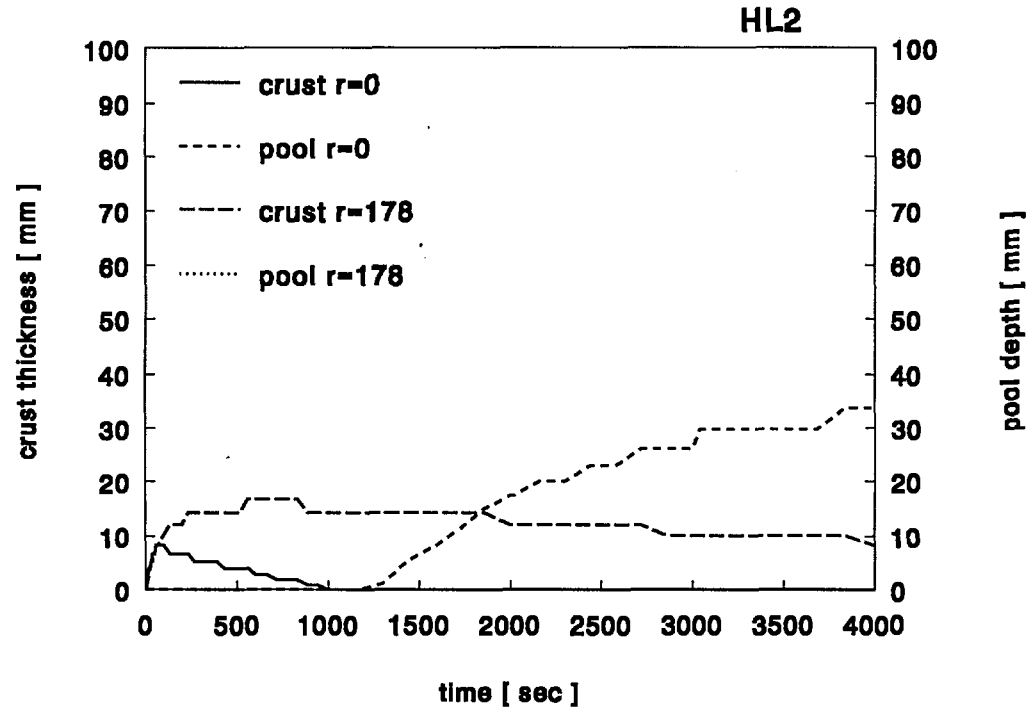

Figure 4.22 *Thickness of the crust and depth of the pool with molten steel at the center line (r = 0 mm) and at a radial distance r = 178 mm for case HL2*

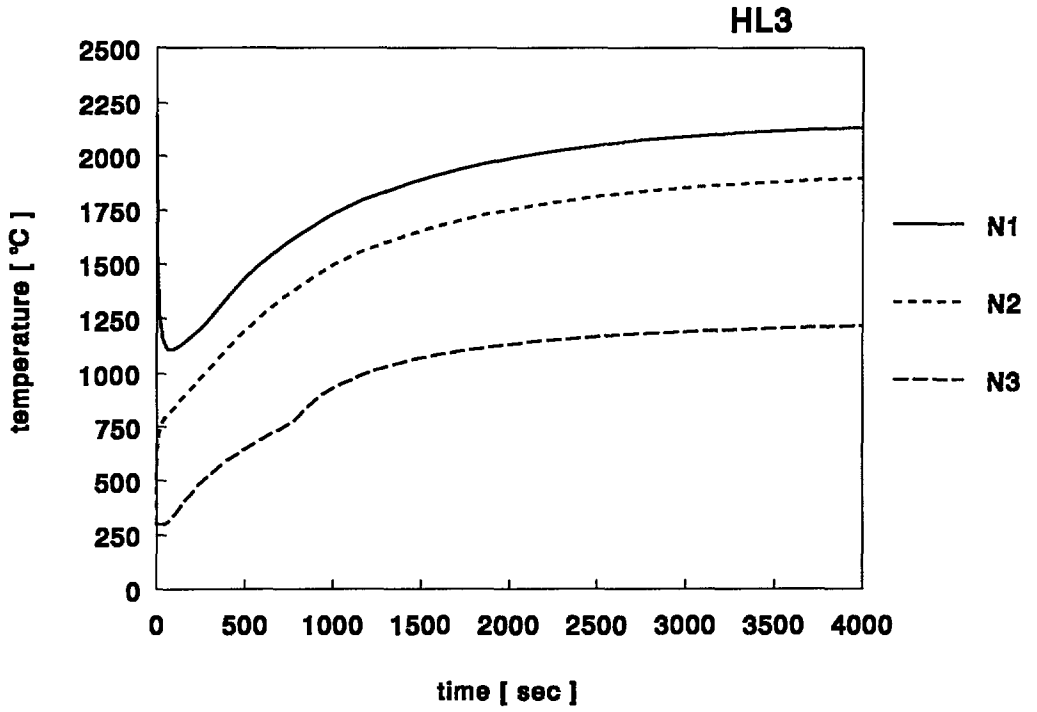

Figure 4.23 *Temperature history for case HL3 at nodes N1, N2 and N3 as depicted in Figure 3.2*

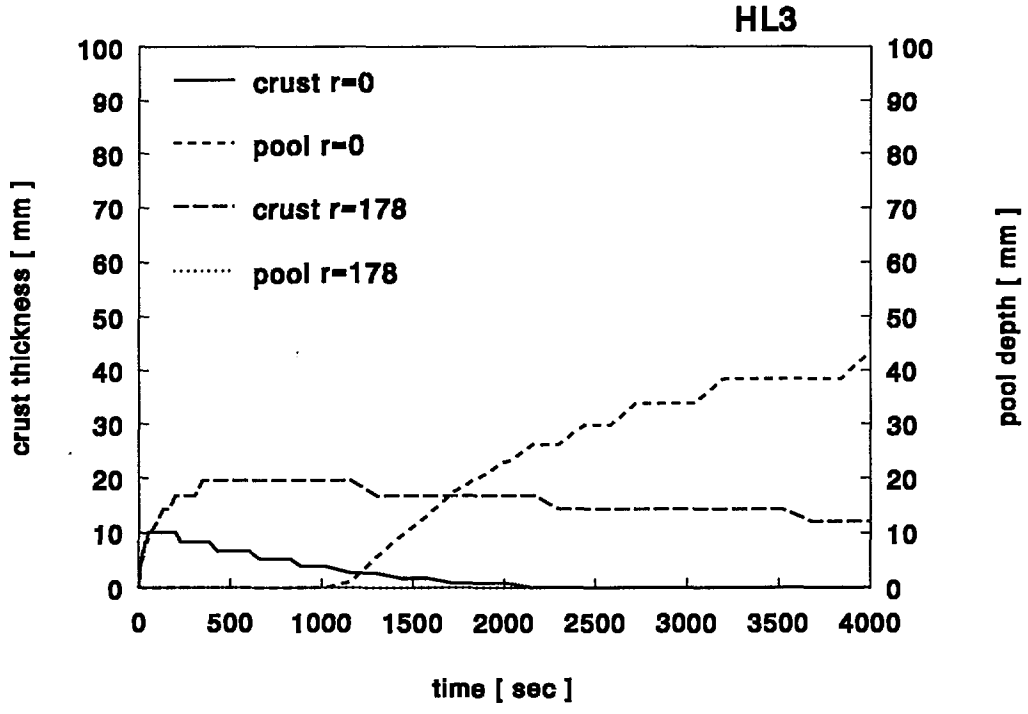

Figure 4.24 *Thickness of the crust and depth of the pool with molten steel at the center line (r = 0 mm) and at a radial distance r = 178 mm for case HL3*

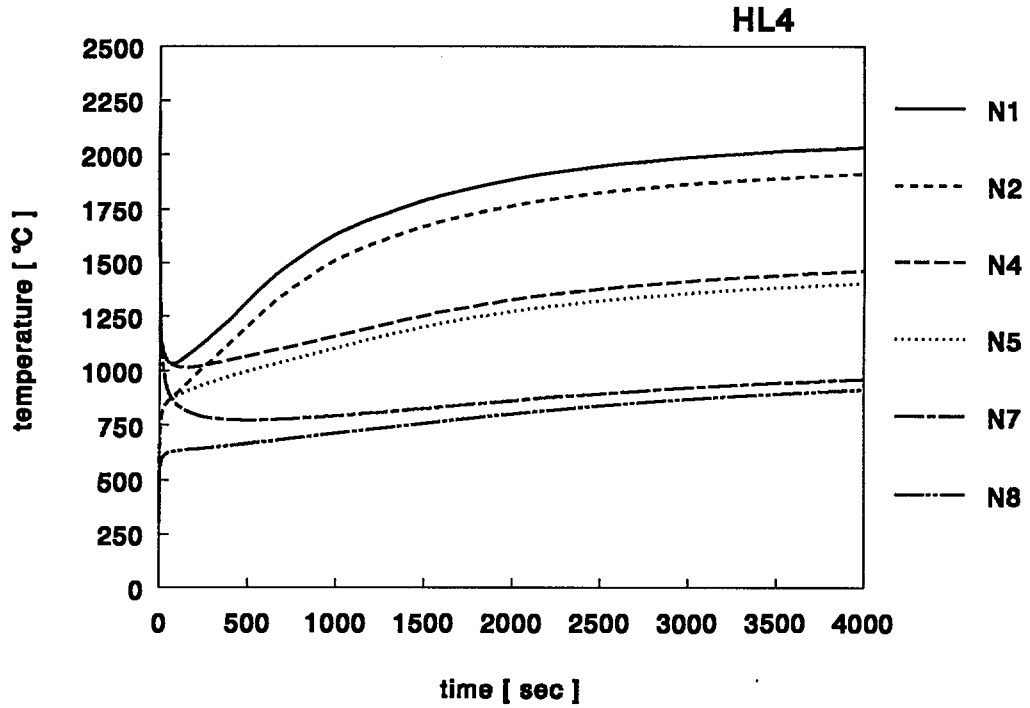

Figure 4.25.a *Temperature history for case HL4 at locations depicted in Figure 3.2*

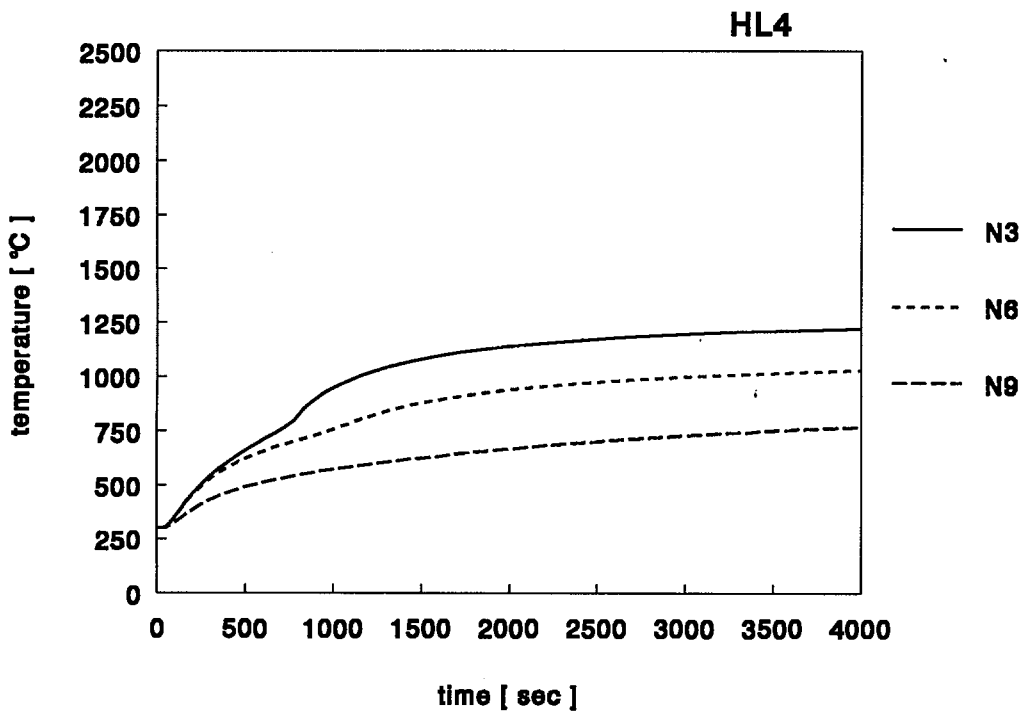

Figure 4.25.b *Temperature history for case HL4 at locations depicted in Figure 3.2*

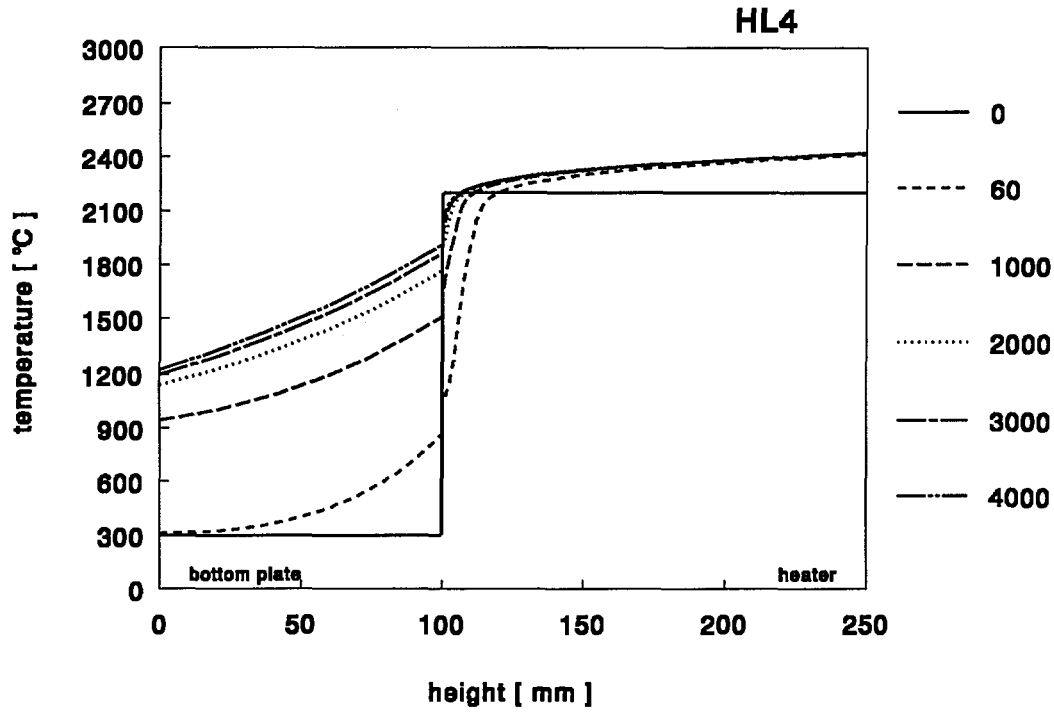

Figure 4.26 *Axial temperature distribution at the center line for case HL4*

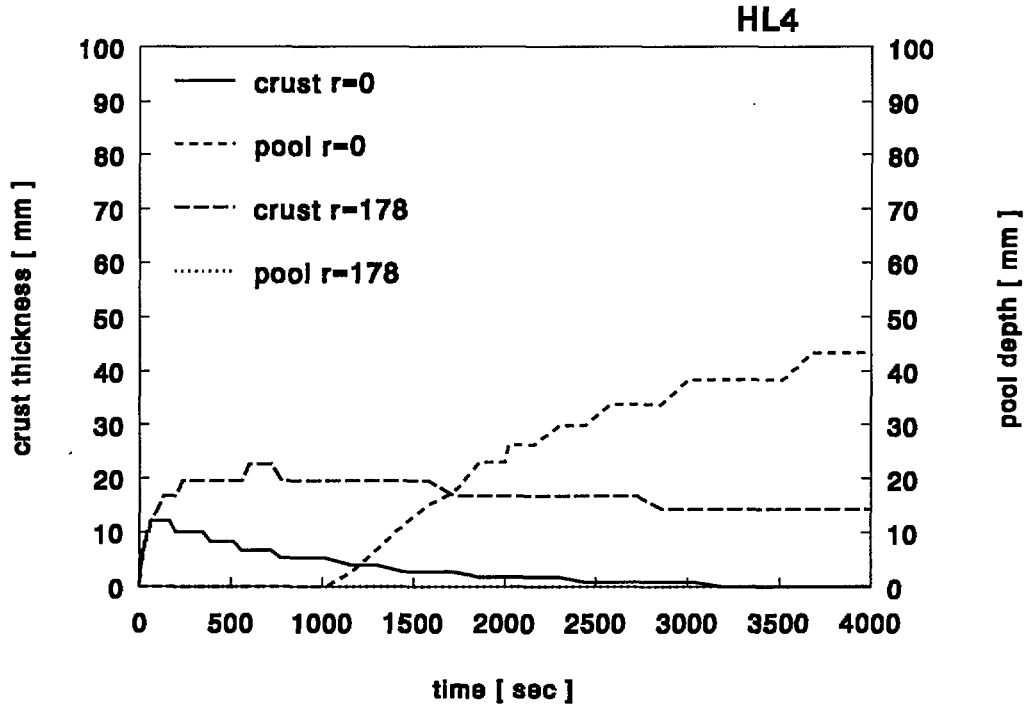

Figure 4.27 *Thickness of the crust and depth of the pool with molten steel at the center line (r = 0 mm) and at a radial distance r = 178 mm for case HL4*

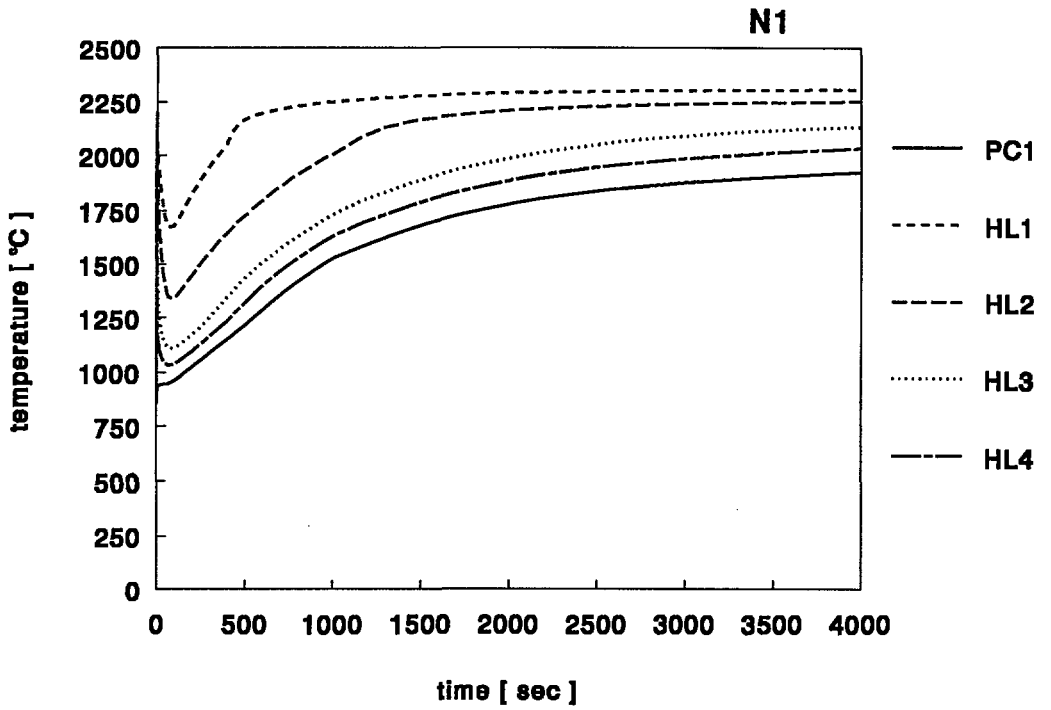

Figure 4.28.a *Temperature history for HL-series and case PC1 at node N1 as depicted in Figure 3.2*

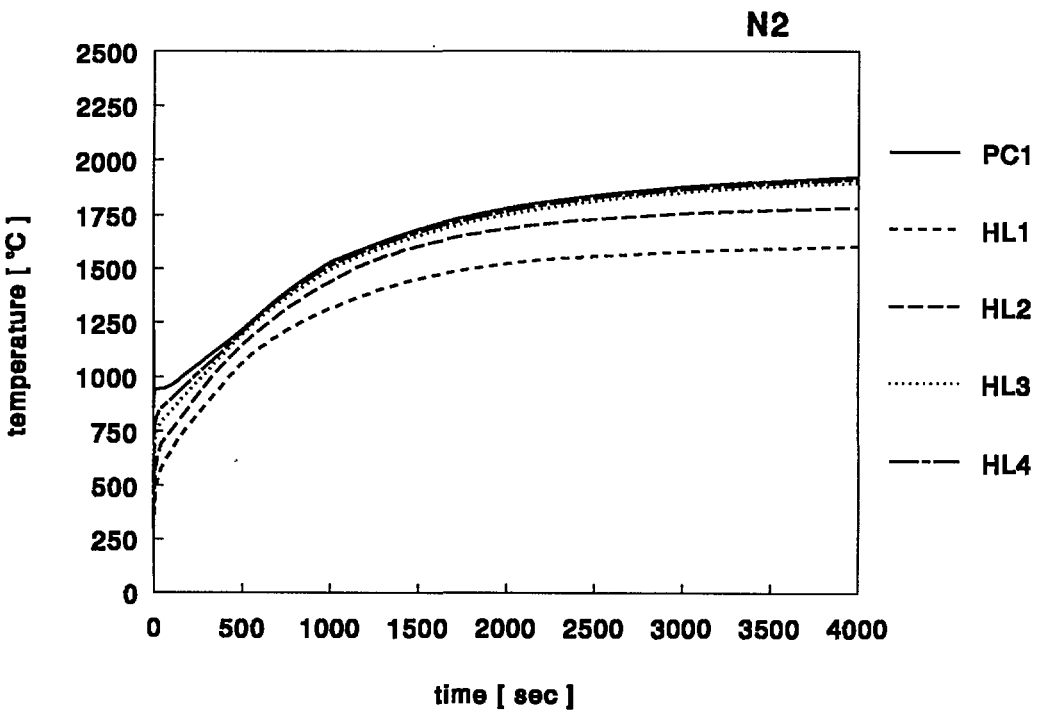

Figure 4.28.b *Temperature history for HL-series and case PC1 at node N2 as depicted in Figure 3.2*

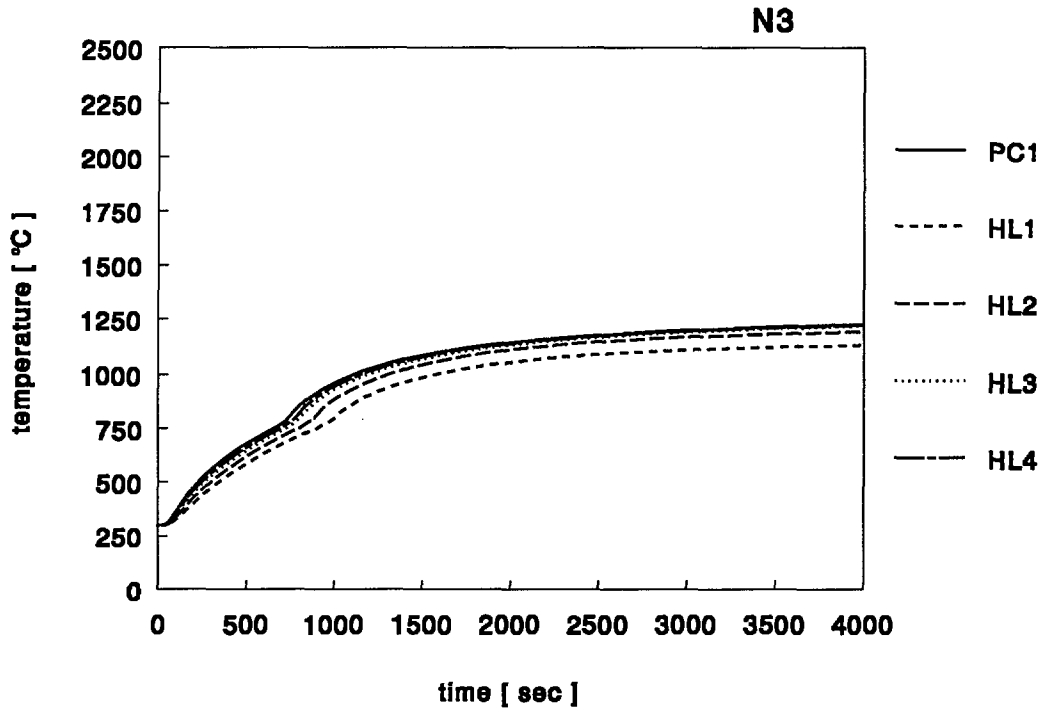

Figure 4.28.c *Temperature history for HL-series and case PC1 at node N3 as depicted in Figure 3.2*

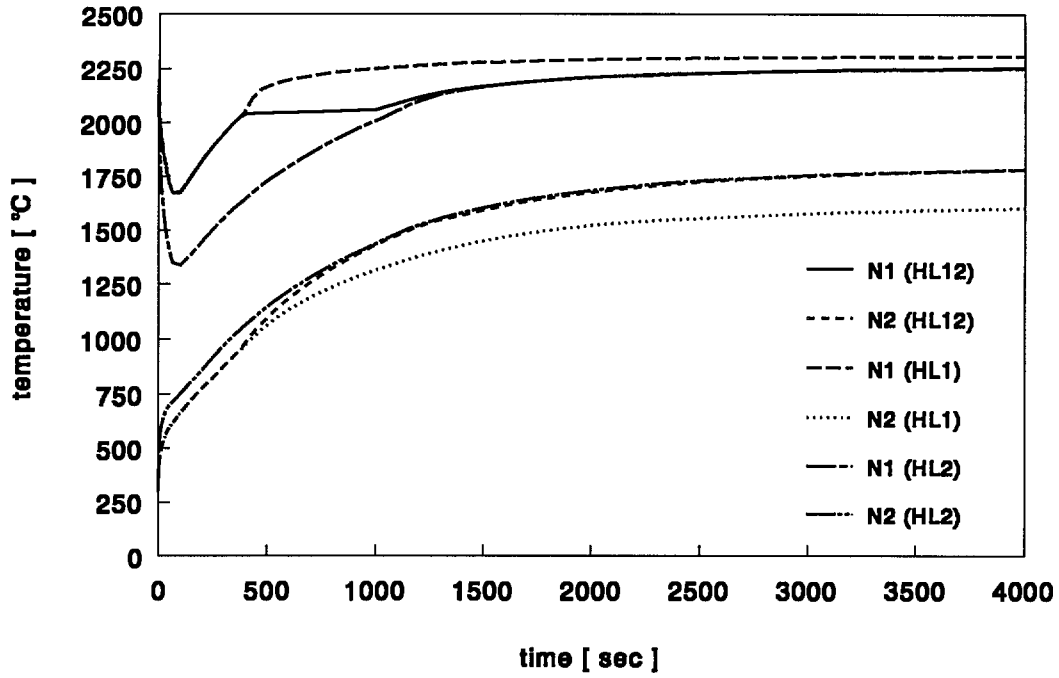

Figure 4.29.a *Temperature history for case HL12, case HL1 and case HL2 at the nodes N1 and N2 as depicted in Figure 3.2*

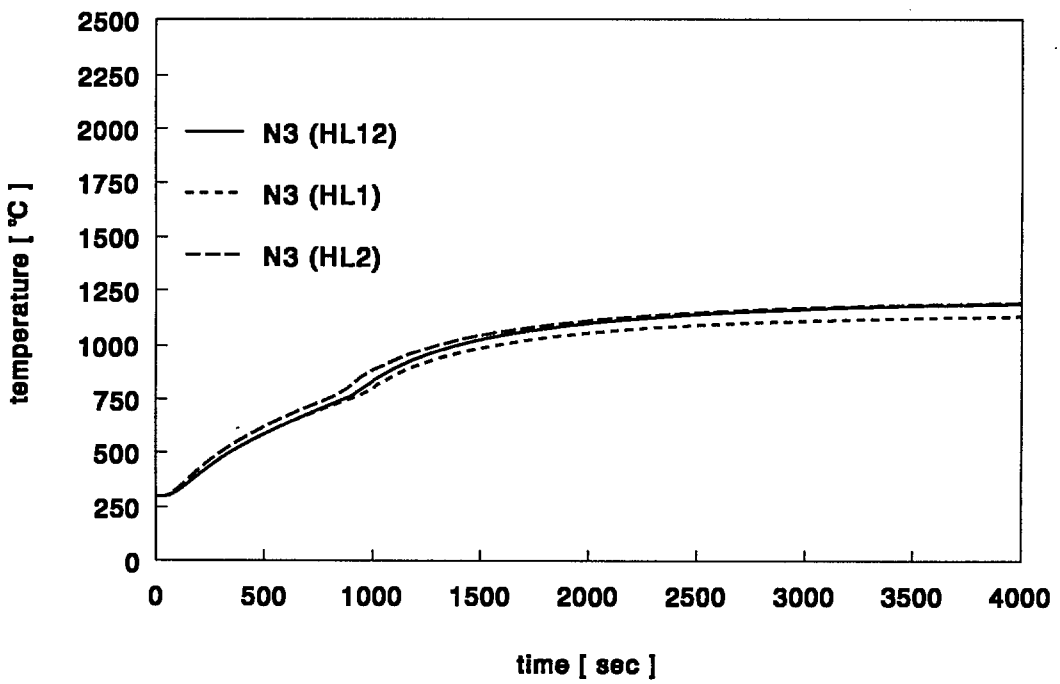

Figure 4.29.b *Temperature history for case HL12, case HL1 and case HL2 at the node N3 as depicted in Figure 3.2*

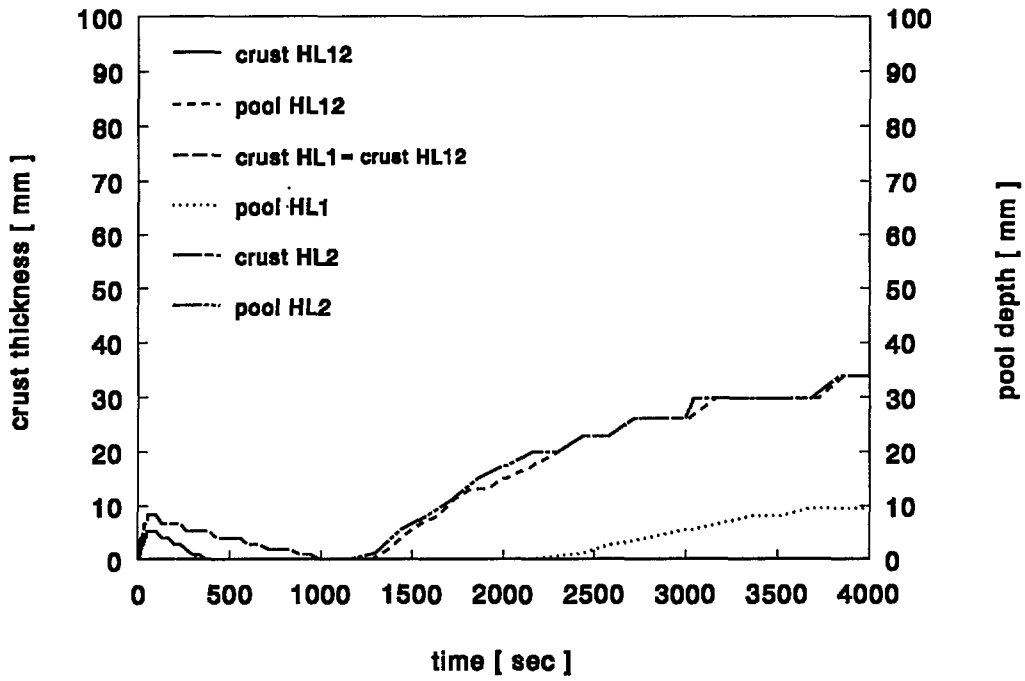

Figure 4.30 *Thickness of the crust and depth of the pool of molten steel at the center line (r = 0 mm) for case HL12, case HL1 and case HL2*

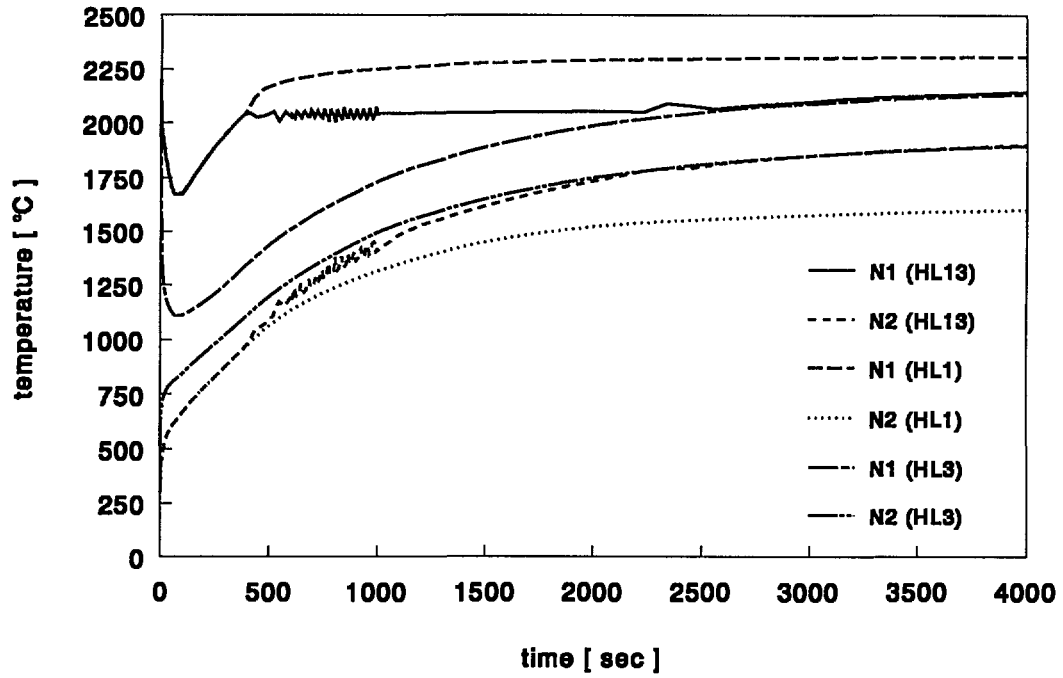

Figure 4.31.a *Temperature history for case HL13, case HL1 and case HL2 at the nodes N1 and N2 as depicted in Figure 3.2*

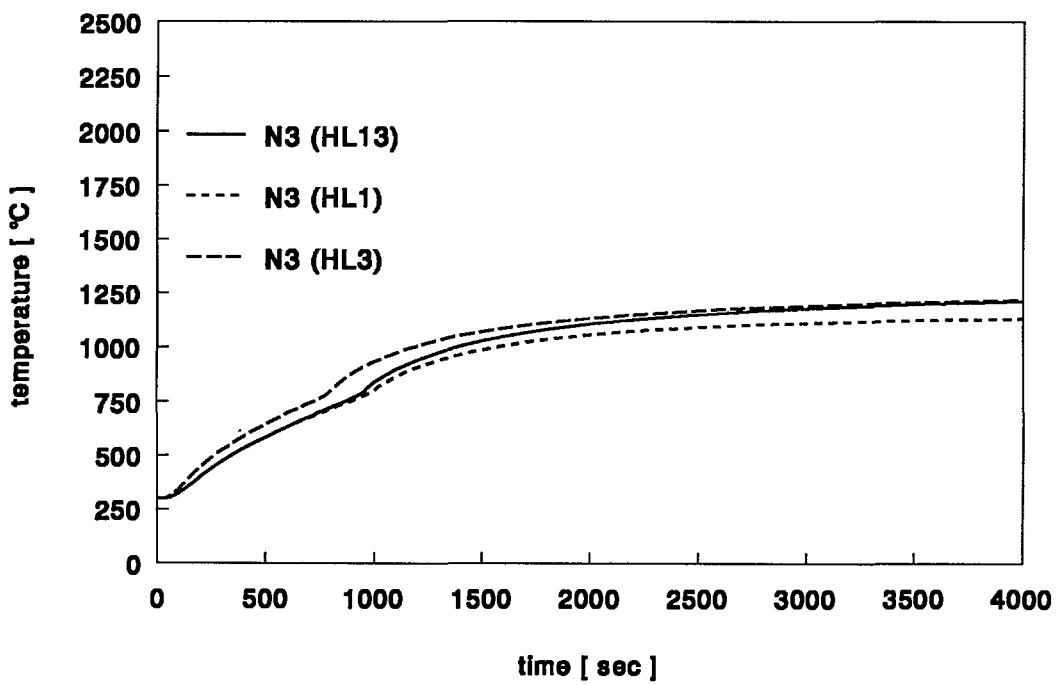

Figure 4.31.b *Temperature history for case HL13, case HL1 and case HL2 at the node N3 as depicted in Figure 3.2*

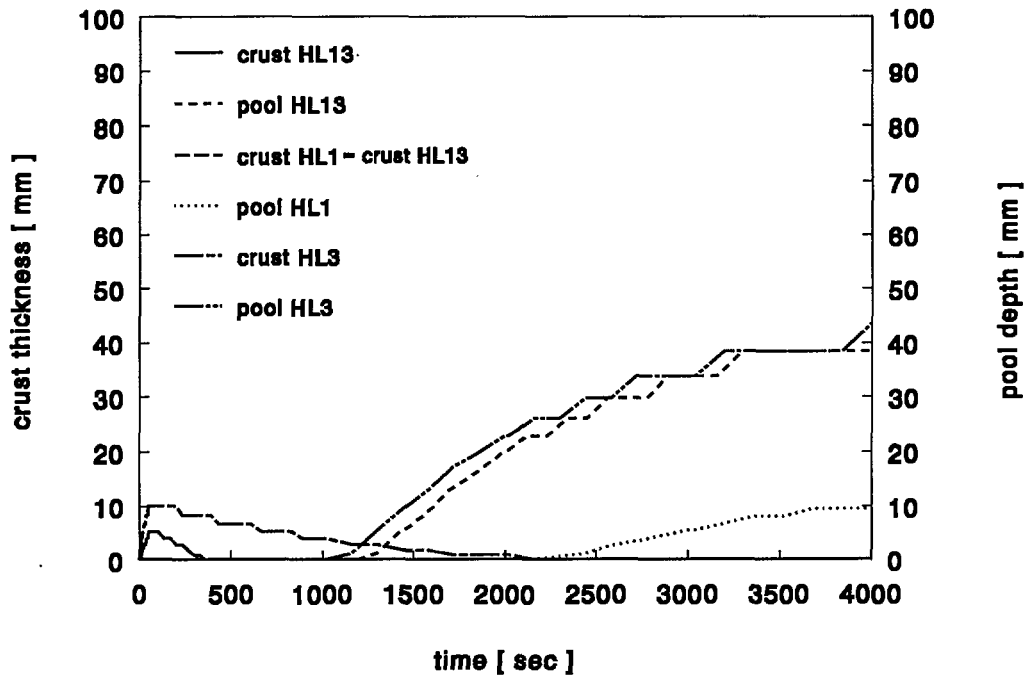

Figure 4.32 *Thickness of the crust and depth of the pool of molten steel at the center line (r = 0 mm) for case HL13, case HL1 and case HL3*

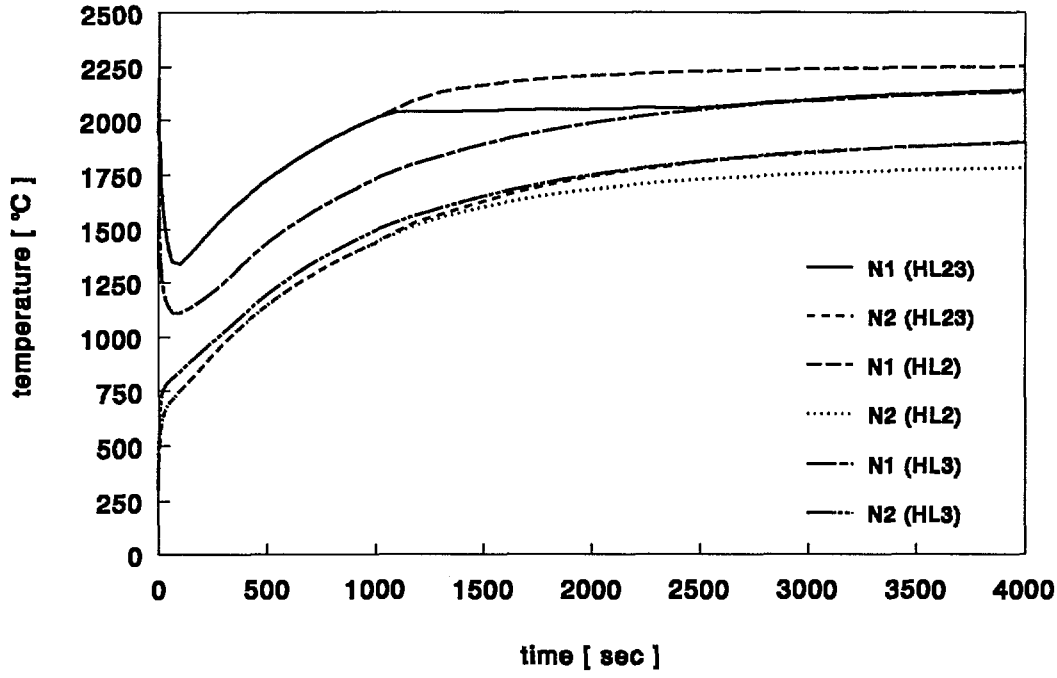

Figure 4.33.a *Temperature history for case HL23, case HL2 and case HL3 at the nodes N1 and N2 as depicted in Figure 3.2*

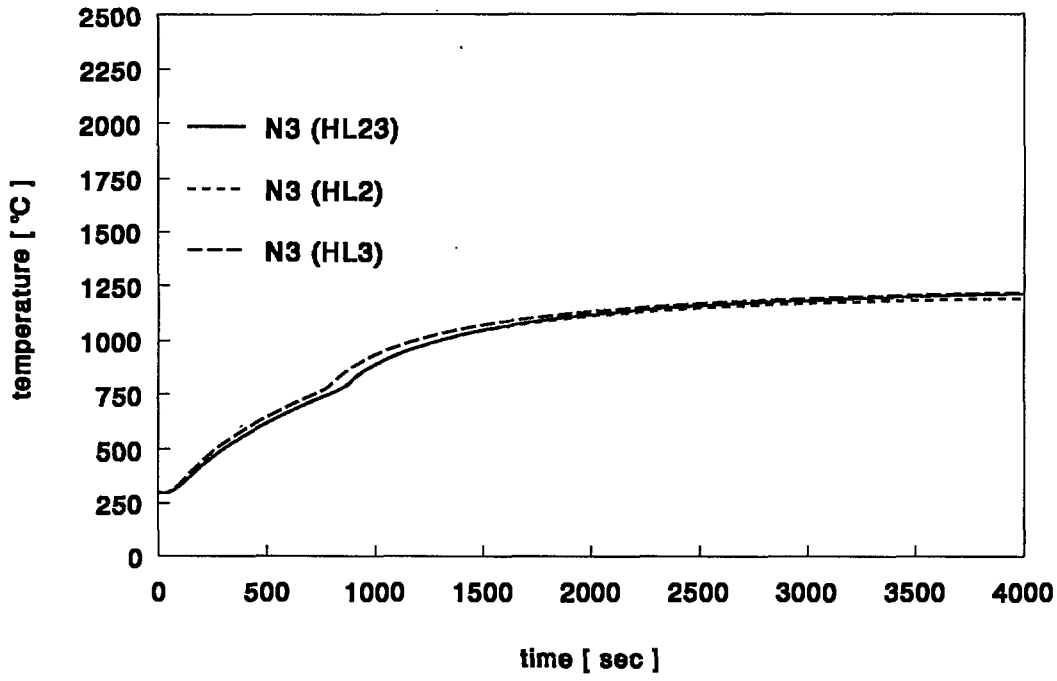

Figure 4.33.b *Temperature history for case HL23, case HL2 and case HL3 at the node N3 as depicted in Figure 3.2*

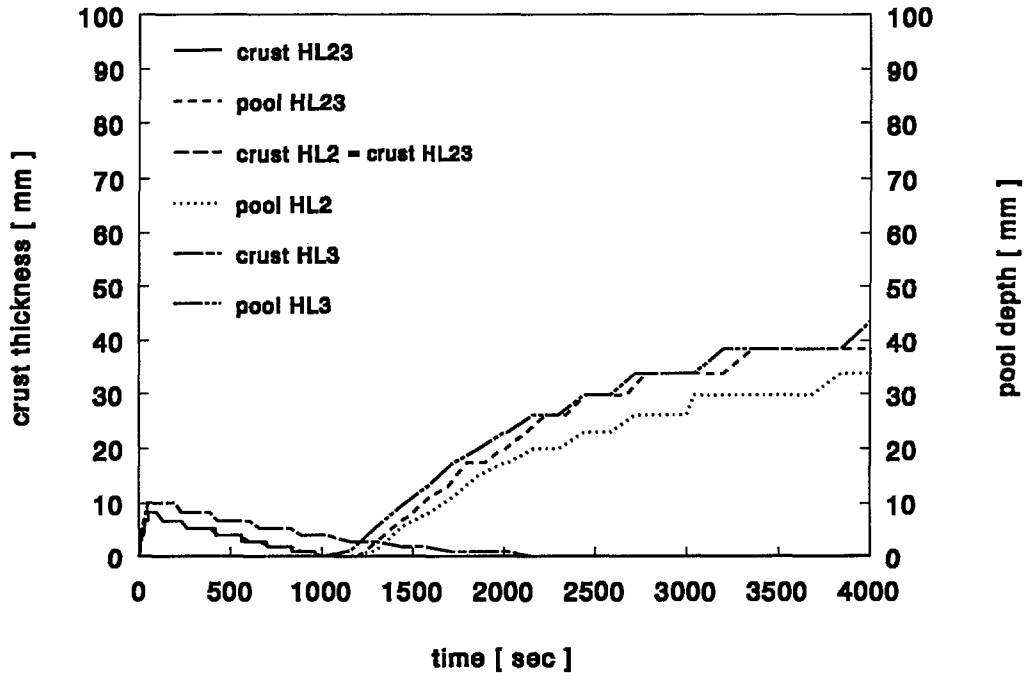

Figure 4.34 *Thickness of the crust and depth of the pool of molten steel at the center line (r = 0 mm) for case HL23, case HL2 and case HL3*

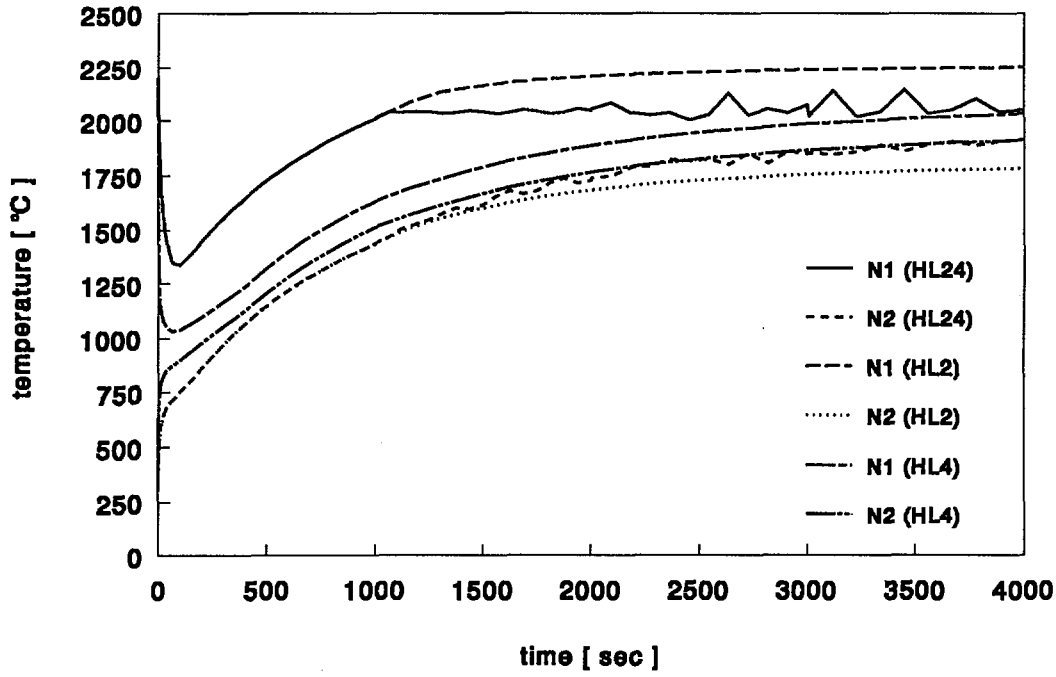

Figure 4.35.a *Temperature history for case HL24, case HL2 and case HL4 at the nodes N1 and N2 as depicted in Figure 3.2*

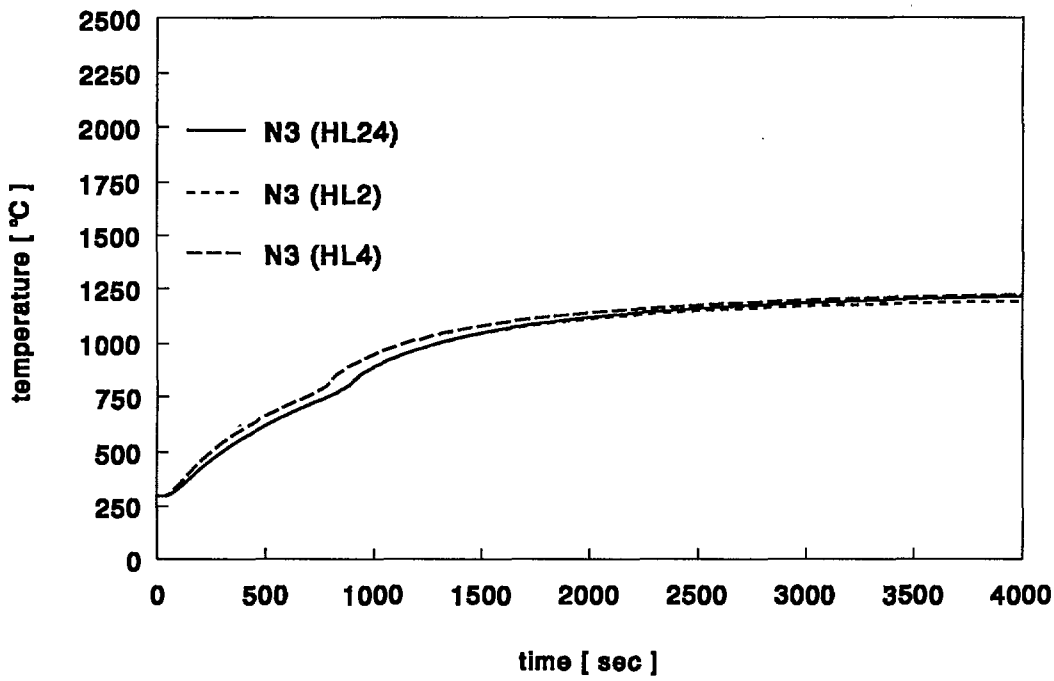

Figure 4.35.b *Temperature history for case HL24, case HL2 and case HL4 at the node N3 as depicted in Figure 3.2*

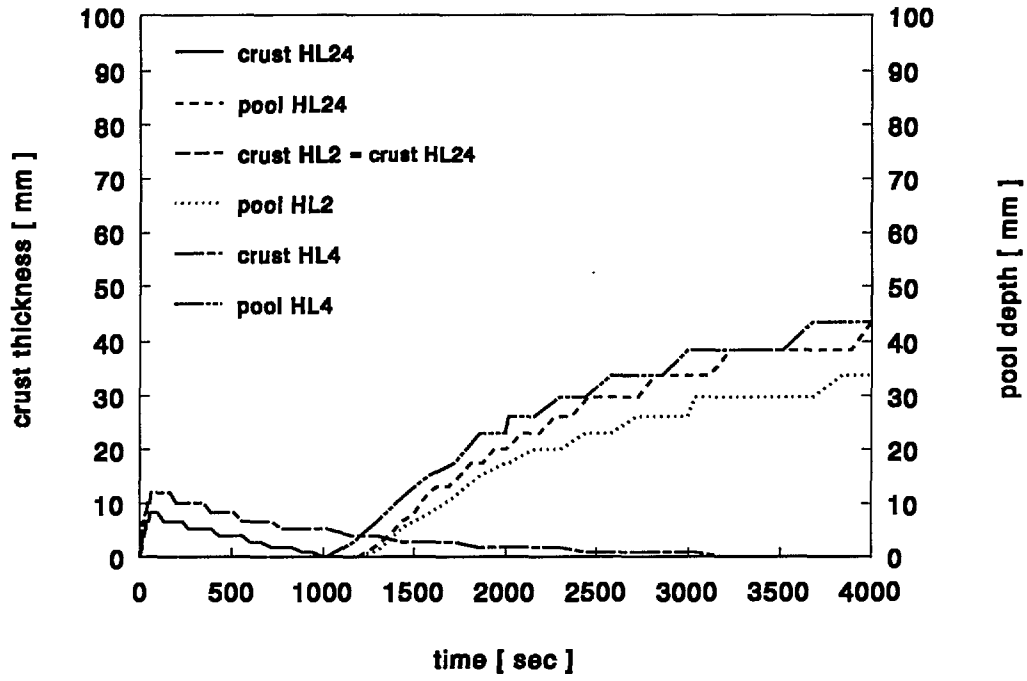

Figure 4.36 *Thickness of the crust and depth of the pool of molten steel at the center line (r = 0 mm) for case HL24, case HL2 and case HL4*

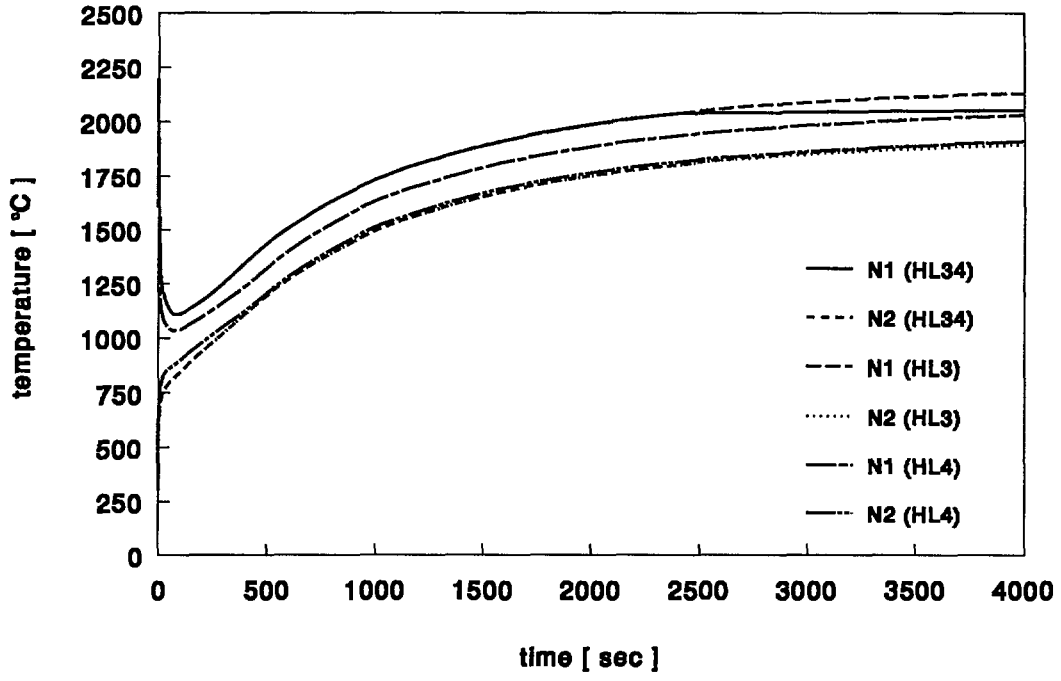

Figure 4.37.a *Temperature history for case HL34, case HL3 and case HL4 at the nodes N1 and N2 as depicted in Figure 3.2*

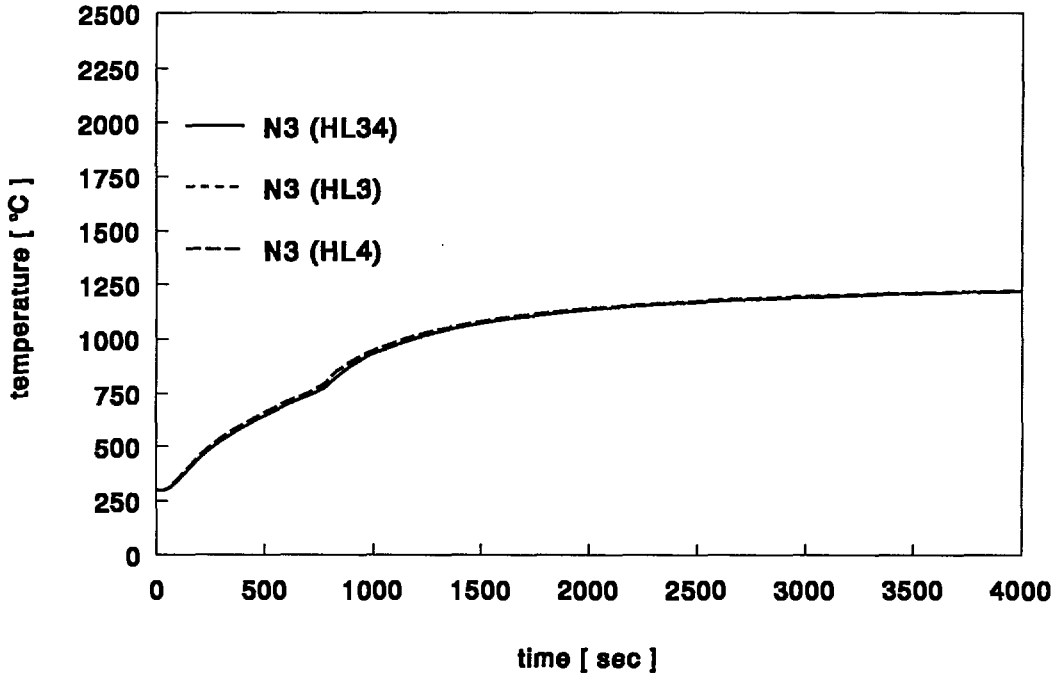

Figure 4.37.b *Temperature history for case HL34, case HL3 and case HL4 at the node N3 as depicted in Figure 3.2*

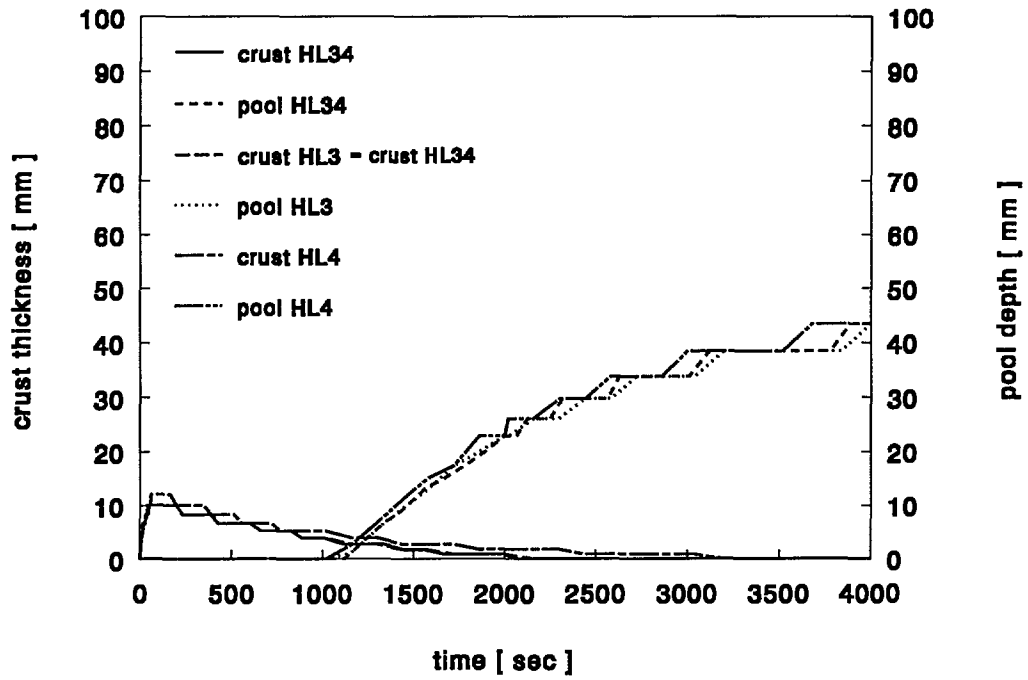

Figure 4.38 *Thickness of the crust and depth of the pool of molten steel at the center line (r = 0 mm) for case HL24, case HL2 and case HL4*